Available online at www.sciencedirect.com
ScienceDirect
Cement and Concrete Research 37 (2007) 414–437
Cement and Concrete Research

Water vapour sorption experiments on hardened cementitious materials Part I: Essential tool for analysis of hygral behaviour and its relation to pore structure

Véronique Baroghel-Bouny *

Laboratoire Central des Ponts et Chaussées, 58 Bd Lefebvre, F-75732 Paris Cedex 15, France

Received 7 September 2006; accepted 17 November 2006

Abstract

This paper forms the first part of a series. In this first part, a broad range of normal and high-performance (HP) hardened cement pastes and concretes is studied under both laboratory and in-situ conditions.

Water vapour desorption–adsorption experiments are carried out by means of the saturated salt solution method on very thin specimens. The effect of various parameters and in particular of the mix-composition is studied on the so-called water vapour sorption isotherms (WVSIs). It is found that the presence of aggregates does not influence the curves. Likewise, the peculiarities of HP materials are highlighted: within the high relative humidity (RH) range, significant lower water contents are measured than for normal materials, and large RH changes induce only slight variations of water content. More generally, desorption isotherms can be partitioned in several ranges, which are influenced or not by W/C: a unique partition is pointed out, valid for every material tested. Moreover, the hysteretic behaviour of the materials is investigated by plotting scanning isotherms within various RH ranges and by performing first and second desorption–adsorption cycles. Furthermore, a pore structure analysis is carried out from WVSIs. The bulk porosity accessible to water, the C–S–H ''gel'' porosity, the BET specific surface area, and the BJH pore size distribution are thus assessed, along with the C–S–H ''gel'' amount. In addition, a master curve is exhibited as regards the average adsorbed water layer thickness *vs.* RH, for RH ≤ 63.2%.

Moisture profiles in structural elements exposed to various drying conditions in laboratory and in natural environments (RC test specimens and bridge deck) are assessed by means of gamma-ray attenuation measurements. A perfect consistence is pointed out between the water contents measured by this technique on 70- to 150-mm thick cylinders and those provided by the desorption experiments previously mentioned (on 1- to 3-mm thick specimens). The very similar moisture profiles and the high degrees of liquid water saturation recorded in HP materials, whatever the mixture, the age and the environmental conditions, confirm that these materials are weakly sensitive to environmental hygral changes within a broad RH range.

Keywords: (B) Pore structure; (C) Water vapour sorption isotherm — hysteresis-moisture profile-drying

1. Introduction

Nowadays, the durability of reinforced concrete (RC) structures is a main concern, since engineers have to take into account the target service life (often over 100 years for many civil engineering structures), when selecting concrete mixtures and designing structures. Durability is determined by the coupled action of various physical and chemical processes, such as carbonation, chloride or sulphate ingress, freezing and thawing cycles, as well as alkali–silica reaction. These processes are not only complex in nature but also capable of evolving with time, especially over the long term. These features make the durability difficult to quantify, and hence the lifetime of RC structures difficult to predict.

Nevertheless, there is a widely recognized feature: these various chemical and physical processes are all dependent on moisture. Numerous examples can be found in the practice and in the research works reported in the literature. As a matter of fact, chloride ions require a liquid phase to penetrate and diffuse in concrete. Conversely, the carbon dioxide gas requires on the one hand a connected gas phase to penetrate and diffuse in the material, since in the liquid phase the diffusion coefficient is 10^4 smaller (10^{-12} against 10^{-8} m^2 s^{-1} in gaseous phase). On the

* Tel.: +33 1 40 43 51 32; fax: +33 1 40 43 54 98.
E-mail address: baroghel@lcpc.fr.

0008-8846/$ - see front matter © 2006 Elsevier Ltd. All rights reserved.
doi:10.1016/j.cemconres.2006.11.019

other hand, the presence of a liquid phase is needed for the carbonation chemical reactions themselves, since dissolution of $Ca(OH)_2$ and CO_2 is required prior to the reaction, which involves the ionic species Ca^{2+} and CO_3^{2-}. This last feature results from the weak probability (for kinetic reasons) of occurrence of the heterogeneous reaction involving directly solid $Ca(OH)_2$ and gaseous CO_2. This yields the existence of a relative humidity (RH) range, where carbonation is favoured (mid RH range, according to [1–3], or high RH range, according to [4]). This has in particular been applied for the development of accelerated carbonation tests. Likewise, it is now well established that the presence of water has a prejudicial effect with respect to various internal concrete degradation processes. This has thus been for example taken into account as a first-order engineering approach in models accounting for the kinetics and the asymptotic behaviour of the alkali–silica phenomenon [5], even if the elementary mechanisms associated with water still remain to be clarified. Note that the evaporable water content evolution in concrete *vs.* time may have an internal origin (the so-called self-desiccation due to cement hydration [6–8]) or/and an external origin (exchanges with the environment, according to weathering conditions). It generates respectively early-age shrinkage and delayed (shrinkage and creep [9]) deformations, along with associated cracking [10–12]. This shows that water solely (without any other species) is likely to impair the mechanical properties and the durability of RC structures. It can be concluded that a correct understanding, prediction and improvement of the behaviour and durability of RC structures unavoidably requires the assessment of the moisture properties of the constitutive cementitious material.

The previous analysis highlights that water vapour desorption and adsorption experiments can constitute an essential tool with respect to RC durability issues. These experiments do allow the assessment of:

- the so-called water vapour desorption and adsorption isotherms (WVSIs), plotting the equilibrium mass water content of the (hardened) material *vs.* RH, at a constant temperature. These data are gas–liquid–solid equilibrium properties and thus quantify the water–solid interactions. In this case, the external RH is equal to the internal one (*i.e.* the RH prevailing in the gaseous phase of the pore network of the material), as the material is in thermodynamical equilibrium with its environment. This curve is also called *integral moisture capacity*. The desorption isotherm can be translated into the capillary pressure curve of the material, which plots the capillary pressure *vs.* the degree of liquid water saturation, and which is involved as a state equation in the modelling of moisture transport [13,14] and of associated phenomena such as drying shrinkage [12,15], or in the modelling of carbonation, for example [3,16,17]. In addition, the adsorption isotherm can be translated into the adsorbed water layer thickness curve, which plots the average adsorbed water layer thickness *vs.* RH, similarly as the ''*t*-curves'' of non-porous adsorbents (see Section 4.4),
- the pore structure characteristics: bulk porosity accessible to water, porosity of calcium silicate hydrate (C–S–H) ''gel'', BET specific surface area, BJH pore size distribution,... (as WVSIs reflect the pore system of the material), as well as the C–S–H ''gel'' amount (see Section 4.4),
- transport properties (permeability and diffusion coefficients, as shown in the second part of the paper series [13]).

Basic physical mechanisms, such as molecular adsorption (/desorption), capillary condensation(/evaporation), surface tension, disjoining pressure,..., which are usually used to analyse sorption data, depending on the pore size range, have been studied for a very long time. In addition, not only empirical formulas but also various physically-based models have been developed worldwide on these bases to account for adsorption isotherms, in order to understand the physics of confined systems and to predict their behaviour. For example, the BET model (derived from the statistical thermodynamics of adsorption) within the low RH range [18], and its numerous extensions (e.g. [19,20]), can be mentioned. More recently, a thermodynamics-based model, which introduces the concept of excess surface work of the adsorbed layer, has been proposed by Adolphs and Setzer [21]. One can also mention the Grand Canonical Monte Carlo simulation study of argon adsorption and capillary phenomena in silica nanopores of different morphologies and topologies by Coasne et al. [22], where the authors also discuss the validity of the BET and BJH methods.

Nevertheless, it is not so easy to find in the literature detailed and comprehensive WVSI data on hardened concretes, and only a few data are available on hardened cement pastes (hcps) or mortars. This maybe results from the fact that the associated experiments can be time consuming (or need sophisticated apparatus to perform ''quick'' tests) and require very accurate testing procedure and experimental conditions. As regards hcps, some of the first results were published by Powers and Brownyard in 1948 [23] and Feldman in 1968 [24]. Other researchers have also more recently published data on this topic, on hcps [25–27], mortars [28–30] or even on ultra-high performance concrete [31]. The first results obtained by the author on hcps and concretes were published in 1993 [32].

The present paper is devoted to the study of the hygral behaviour of hardened cementitious materials and its relation to pore structure, in both laboratory and natural environments. In order to easily transfer the research work to the practice, the purpose is here to:

- use tools as simple as possible,
- be in conditions as close as possible to that of concrete in field conditions,
- provide data likely to be immediately and directly included in physically and chemically based macroscopic models.

A broad range of normal and high-performance (HP) cement pastes and concretes is studied, from hydrated synthesised C_3S to concrete mixtures actually used in bridges. In this first part, WVSIs are measured and analysed. The results deduced from WVSIs with respect to pore structure characteristics are also analysed. The deduced results with

Table 1
Mix-composition and main characteristics of the concretes

Series (cement) reference	1	2		3			4
Material reference	B	BO	BH	M25	B80-S	M75-FS	B30-A
Gravel (G) content (in kg.m^{-3}) (min/max grain size in mm)	1150 (8/16)	1192 (4/20)	1265 (4/20)	1007 (5/20)	980 (6/14)	1044 (5/20)	1075 (4/20)
Sand (S) content (in kg.m^{-3}) (min/max grain size in mm)	675 (0/2)	744 (0/5)	652 (0/5)	899 (0/5)	790 (0/4)	877 (0/5)	764 (0/4)
Cement (C) content (in kg.m^{-3})	400	353	421	230	420	360	350
Silica fume (SF) content (in kg.m^{-3})			42.1		35	22	
Water (W) content (in kg.m^{-3})	180	152	112.3	193	147	136	175
Superplasticizer content (in kg.m^{-3})			7.59		7.28	12.0	
Water-to-cement ratio (W/C)	0.45	0.43	0.27	0.84	0.35	0,38	0.50
Water-to-binder ratio (W/B)	0.45		0.24	0.84	0.32	0.36	0.50
Silica fume to cement ratio (SF/C)			0.10		0.08	0.06	
Gravel-to-sand ratio (G/S)	1.7	1.6	1.9	1.1	1.2	1.2	1.4
Degree of hydration of the cement α (−) after sealed curing *(age = 6 months — 1 year)*	–	0.92 [a]	0.75 [b]	–	0.75 [a]	0.75 [a]	–
28-day cylinder average compressive strength (in MPa)	–	49.4	115.5	25.1	85.3	85.5	37.5

[a] Measured by thermogravimetric analysis.
[b] Mean value between XRD diffractometry and thermogravimetric analysis [33].

respect to transport properties are presented in the second part of the paper series [13]. The similarities and the discrepancies between the different materials are investigated, in particular the influence of mix-parameters such as the water-to-cement ratio (W/C). The possibility to assess intrinsic data and master curves is explored. The hysteretic behaviour of the materials and the effect of the test temperature are also studied. Moreover, water vapour sorption data are used to explain the long-term drying behaviour of test specimens and structures exposed to various laboratory and natural environments.

2. Materials tested

2.1. Set of cement pastes and concretes studied in laboratory

Several cement pastes (referenced C, CP, CN, CO, and CH) and concretes (referenced B, BO-AF, BO-SN, BO, BH, M25, B80-S, and B30-A) with:

- various type-I OPCs (CEM I — 52.5, according to the EN 197-1 European standard),
- a broad range of water-to-cement ratios: W/C ranges from 0.20 to 0.84,
- possible incorporation of silica fume (SF): SF/C ranges from 0 to 0.10,

have been studied in laboratory.

The mixture proportions and the main characteristics of the concretes and the cement pastes are summarized in Tables 1 and 2, respectively. The mixtures are separated in 5 series. For a given series, the constituents (cement, silica fume, and aggregates) are the same. The aggregates were dried before mixing. The mineralogical composition, calculated by Bogue′s formula from the chemical composition, and the Blaine fineness of the cements used are given in Table 3. Some of the mixtures (CH, BH, and B80-S) are HP materials: they are prepared with a low W/C, with silica fume, and with superplasticizer. The silica fume was added as dry powder. The chemical composition of the silica fumes used and their BET specific surface area (measured by nitrogen adsorption) are given in Table 4. Note that the mixture B80-S has been used for the building of a bridge in France (‘‘Sens Bridge’’): the sorption experiments (see Section 3) were therefore performed on specimens prepared from cores extracted from the inner zone of this bridge.

The concretes BO-AF and BO-SN (series 2*) are not reported in Table 1, since their constituents and mix-composition are similar to those of BO (series 2). Only the cement (see Table 3) and the initial water content are slightly different. The respective W/C are 0.49 and 0.44. Moreover, a fully hydrated synthesised C_3S (W/C around 0.50) and a fully hydrated white cement (see Table 3) paste with W/C around 0.55 (referenced PCB) have been tested for comparison with the other materials. These materials were prepared by means of a specific procedure (casting–hardening–crushing–casting–compression), in order to favour full hydration. For these materials, the degree of hydration of the cement was estimated to be 0.98 on the basis of microscopic investigations carried out before sorption experiments [35].

2.2. Concretes studied under in-situ conditions

Concretes M25 and M75-FS (HPC) from series 3 (see Table 1), mixed with same constituents, have been studied under in-situ conditions, in ‘‘Melun’’ and ‘‘Maurienne’’ exposure sites in France (RC structural elements, see Section 5 and [37–39]). The HPC of the deck of the ‘‘Ré Island Bridge’’ (referenced B60-FS: CEM I 52.5 ; W/C = 0.38 ; SF/C = 0.075 ; 28-day cylinder average

Table 2
Mix-composition and main characteristics of the cement pastes

Series (cement) reference	1	2			
Material reference	C	CP	CN	CO	CH
Water-to-cement ratio (W/C)	0.45	0.60	0.45	0.35	0.20
Water-to-binder ratio (W/B)	0.45	0.60	0.45	0.35	0.18
Silica fume to cement ratio (SF/C)					0.10
Degree of hydration of the cement [a] α (−) after sealed curing *(age = 2 years)*	–	0.92	0.85	0.75	0.48

[a] Mean value between BSE-SEM image analysis and thermogravimetric analysis [33–36].

Table 3
Mineralogical composition and Blaine fineness of the cements

	Content (%)								Blaine fineness ($m^2\ kg^{-1}$)
Series	C_3S	C_2S	C_3A	C_4AF	gypsum	$CaCO_3$	free CaO	Alkalis	
1	39.3	35.5	9.7	7.1	6.2	0.52	0.76	Na_2O=0.18 K_2O=0.44	319
2	57.3	24.0	3.0	7.6	4.4	1.8	0.53	Na_2O=0.43 K_2O=0.43	317
2*	63.9	15.0	3.8	5.4	4.8	2.7	0.99	Na_2O=0.19 K_2O=0.26	320
3	57.6	17.8	2.2	12.6	6.2	2.0	0.71	Na_2O=0.12 K_2O=0.30	355
4	59.1	14.5	9.1	9.0			0.97	Na_2Oeq.=0.81	353
white cement	66.5	12.1	10.4	1.0				Na_2O=0.07 K_2O=0.07	

compressive strength=68.0 MPa) has also been studied for comparison (see Section 5 and [39]). Details on the mixtures, the sites, and the RC structural elements or the bridge can be found in the mentioned references.

3. Description of the water vapour sorption experiments

3.1. Experimental procedure: the saturated salt solution method

Various methods can be used for the assessment of WVSIs: the flow division method that mixes dry and saturated air, the method altering temperature or pressure or both, the volumetric method that isothermally changes the vapour pressure in a vacuum system, and gravimetric methods [40]. Most of these methods are rather used in chemistry and physics laboratories. Here, water vapour desorption and subsequent adsorption experiments have been performed by means of the saturated salt solution method [28,33,41], which belongs to the gravimetric type, at a constant temperature and at the atmospheric pressure, on thin specimens of hardened cement pastes and concretes (see [33] for more details).

The experiments consist in enclosing the specimens in sealed cells (desiccators), where the relative humidity is kept constant by means of a saturated salt solution (or silica gel), and in submitting these specimens to step-by-step desorption and subsequent adsorption processes (stepwise changes in RH). The desiccators are laid in a thermo-regulated bath at $T=23\pm0.1$ °C (or in an oven at $T=44\pm0.1$ °C, in the case of concrete BO-AF). The desiccator volume is high enough, compared to the volume and the number of specimens, in order that the specimen load doesn't disturb the ambience controlled by the saturated salt solution and does not delay the set up of equilibrium. The total gas pressure of the cell is not imposed. It is therefore assumed to be equal to the atmospheric pressure during the whole experiment. In the test conditions (0.1 °C temperature stability, pureness of the salts used, early preparation of the solutions,…), it can be assumed that the RH precision is 0.1%.

The mass water content of the specimens is determined by weighing. After removing the small upper stopper of the desiccator, each specimen is hung inside the desiccator from the bottom hock of an electronic balance. The precision of the balance is 0.001 g. Since the desiccator is not completely open during the weighing procedure, its ambience and the specimens themselves (as regards hygral state and occurrence of carbonation likely to affect the results [28,33,42,43]) are only slightly disturbed [33]. Each RH step lasts until moisture ''equilibrium'' is reached inside the specimen (see Section 3.5). The mass water content (at ''equilibrium'' state) of the material at the (constant) test temperature can thus be plotted *vs.* RH.

The saturated salt solution method is particularly suitable to concrete specimens and to the study performed here. This is probably the single method, which meets all the following requirements:

- no external pre-drying (that might damage the microstructure),
- no constraint as regards the initial and final (RH) values of the cycles and their magnitude (most of the other techniques only work with previously dried out specimens), as well as the number of cycles. It is therefore possible to investigate drying-wetting cycles (so-called scanning isotherms) and the hysteretic behaviour of the material within various RH ranges (selected according to practical concerns),
- no constraint as regards the duration of each RH step,
- no constraint as regards the specimen size and mass, which offers in particular the possibility to test concrete specimens (most of the other techniques require finely crushed specimens in small quantity, which can affect the results, see for example [44] and Section 3.2),
- reliability over the very long term,
- simple test procedure and cheap set-up.

In addition, this method is often considered as a standard (reference) method. Moreover, as this method provides desorption and adsorption kinetics (relative mass variations *vs.* time), it allows the assessment of additional parameters useful for various durability issues (see for example [13,45]). The fact that the saturated salt solution method is a discontinuous method can appear as a drawback. But this method provides easily a dozen of (RH) plots, which prove to be sufficient to draw, to fit accurately and to analyse the WVSIs, as it will be illustrated in the next sections of this paper and in the

Table 4
Chemical composition and BET specific surface area (measured by nitrogen adsorption) of the silica fumes

	Content (%)							$S_sBET\ (N_2)$ ($m^2.g^{-1}$)
Series	SiO_2	Al_2O_3	Fe_2O_3	MgO	MnO	CaO	Alkalis	
2	87.0	0.27	0.67	1.56	0.07	0.37	Na_2O=0.70 K_2O=2.35	17.6
3	96.0	0.18	0.55	0.65	0.13	0.22	Na_2O=0.25 K_2O=1.05	16.2

second part of the paper series [13]. Finally, its single drawback is the test duration (see Section 3.5). This explains that rapid methods have been developed recently to assess WVSIs or sorption kinetics [27,31,44].

3.2. Specimens

As regards the specimen dimensions, note that sorption experiments don′t require to insure representativeness of concrete, as aggregates don′t play any role in the sorption process (see Section 4.1). Therefore, very thin specimens are used here, in order to be able to reach ‘‘equilibrium’’ (see Section 3.5) in the test conditions. Most of the concrete specimens are 3-mm thick slices, with a diameter within the range 70–110 mm and a mass between 20 and 40 g, depending on the mixture. Some thicker specimens were also tested (thickness around 5 mm, and weight between 50 and 100 g). Hcp specimens are 2- or 3-mm thick slices, with a similar diameter as concrete specimens or a significantly smaller one (25 mm), or crushed slices ($0.8 < d \leq 1$ mm, where d is the mean piece size) laid in stainless steel baskets. Crushing to smaller sizes could induce artefacts [26,33,44]. The mass of most of the crushed hcp specimens is around 8 g.

3.3. Initial state and sorption sequences

The slices were wet sawed from cylinders, after sealed or wet curing.

Stable materials, from a chemical point of view, are required, in order to be able to quantify ‘‘pure’’ physical effects, not affected by chemical reactions during the sorption experiments. Except carbonation, delayed hydraulic or pozzolanic reactions (in the presence of SF) are likely to change the microstructure during the test and hence the WVSIs. For example, when young cementitious specimens are exposed to drying (desorption) and then to very high RHs (in the course of adsorption), delayed chemical reactions can induce irreversible changes and associated consequences such as a second desorption curve which significantly diverges from the first one and an enhanced hysteresis between desorption and adsorption [33,46]. This phenomenon can occur even with mature materials under certain circumstances, in the case of sealed curing. In order to meet as far as possible in the test conditions the chemical stability requirement, the sealed or wet curing lasted between 6 months and 1 year depending on the mixture, given the long duration of the chemical reactions and of the water sorption processes. At this time, very slow kinetics are expected for the chemical reactions, due to the lack of water, available space (for dissolution of reactants and precipitation of hydration products) or unreacted cement amount, depending on the mixture, and a very slight further evolution of the degree of hydration of the cement is expected from this age, as illustrated in [33–36]. The cement hydration (and pozzolanic) processes can therefore be assumed as negligible for the whole duration of the desorption–adsorption test, at least before re-exposure to RH $\geq$97% in the case of sealed-cured materials. The degrees of hydration of the cement, measured after sealed curing for some of the materials tested here, are reported for a given age in Tables 1 and 2 as an example (see [33–36] for other ages and the description of the measuring methods).

The sorption experiments start here by a desorption process, since in field conditions real concrete structures undergo external drying from their virgin state (*i.e.* from the time when the formworks are removed, after casting and curing). Such a procedure provides in addition a first desorption curve that is representative of the virgin material (*i.e.* without any external pre-drying). Note however that the curing conditions can influence (the high RH range of) this curve (possible self-desiccation effects [6–8,36] or possible surface re-hydration in particular in the case of crushed specimens since the crushing process may increase the exposed surface of unreacted grains [33]). The mentioned effects will depend on the mixture and on the starting (RH) point of the first desorption. After this first step-by-step desorption process, some of the materials were submitted to a subsequent step-by-step adsorption process, a second desorption process,… Various RH values were selected as the starting points of the first and subsequent desorption and adsorption processes. Thus, scanning sequences and desorption–adsorption cycles were performed within different RH ranges and after various hygral histories. In particular, cycles were performed within the high RH range, since 70% is the average RH value for most of the environments of RC structures in European countries. The purpose was to study the hysteretic behaviour and the effect of various parameters within these ranges.

3.4. ‘‘Dry’’ standard (reference) state

The choice of the ‘‘dry’’ reference state is of major importance, as it is in particular used for the water content calculations: a change in the method used to obtain this state may induce large changes in the isotherms, as illustrated in [47], where significant higher water contents were observed when the hcps were oven dried at T=105 °C instead of dried by the method used here (see below). Likewise, changes may be recorded in the pore structure characteristics derived from WVSIs (according to the method described in Section 4.4), similarly as in the case of nitrogen sorption [48,49] or mercury intrusion porosimetry (MIP) [50,51] results.

The ‘‘dry’’ reference state is defined here as the ‘‘equilibrium’’ state reached at RH=3% (at the test temperature) after step-by-step desorption. On the basis of experimental results obtained with M25, B80-S, CN and CO, when this ‘‘dry reference state is used an average relative difference of 13.5%, with respect to the water content obtained after oven drying at T=105 °C, can be assumed. The specimens are laid in this case in desiccators, which contain virgin silica gel. It is the lowest RH the specimens are subjected to during the test. This choice avoids submitting the specimens to any more or less controlled drying process carried out in different conditions from that of the isothermal desorption process carried out here (e.g. oven drying at high temperature and in non-controlled RH conditions). Here, the same temperature is maintained during the whole sorption test, including the ‘‘dry’’ state. In addition, the

drying method used here is milder than freeze-drying, than the more conventional D-drying (in dry air at a dew point temperature of −76 °C), than oven drying at $T=105$ °C until constant mass, or than equivalent ones. These last drying procedures are more likely to remove strongly bound interlayer water from the C–S–H, and therefore to induce collapse of pores and modification of the stoichiometry and of the density of the C–S–H [52,53].

Note that the choice of thin specimens, of avoiding external pre-drying, of varying the surrounding RH slowly and gradually, allows to significantly reduce cracking during the sorption process.

3.5. ''Equilibrium'' state and kinetic aspect

Each experimental plot of WVSIs must correspond to an equilibrium state between the pore gaseous phase and the environmental conditions (RH and temperature). To assess valuable WVSIs, it is therefore necessary to take into account the very slow kinetics of moisture transport in mesoporous media such as cementitious materials, where the transport process is further slowed down by water–matrix interactions. Here, a so-called ''equilibrium'' state is assumed when the specimen mass is stabilized for several weeks, at the precision of the measurement (0.001 g). The time required to reach moisture ''equilibrium'' depends in particular on the specimen thickness, the RH gradient, the hygral history and the mixture [33,54–56]. Moisture ''equilibrium'' was not reached before several months in the 3-mm thick specimens tested here at the atmospheric pressure. It has even been reached after more than 1 year in some cases [13,33,54] (see also [29]). Therefore, the results presented in Section 4 are the results of several-year experiments. If ''equilibrium'' is not reached, WVSIs will be wrong, as well as the pore structure characteristics eventually derived from them. In some RH ranges the error can be particularly significant. This is shown in [33] by the desorption isotherms of CO, CH, BO and BH drawn after various durations of the RH steps and by the deduced relative errors *vs.* RH with respect to the values obtained at ''equilibrium'' (see also [29]). Hence, it is not relevant to select *a priori* the duration of the RH steps, in particular if this duration has to be the same for each step and every mixture.

Note that the kinetics would be faster, if the specimens were exposed to pure water vapour in an automatic set-up or to saturated salt solutions under low gas pressure instead of atmospheric pressure. As a matter of fact, in pure water vapour, no molecular water vapour diffusion according to Fick′s law in the gas mixture can occur; the transport is controlled by the total pressure difference (Darcy's law) for both the vapour and the liquid phases inside the material. Further, as the viscosity is lower for the vapour phase than for the liquid phase, if a low RH value is imposed at the boundary, the water vapour transport according to Darcy′s law will be prominent. In this case, the rate is significantly greater than that of moisture transport in the presence of dry air at atmospheric pressure. Vacuum or low gas pressure are also effective in preventing carbonation. Nevertheless, they were not applied here, as the aim was to analyse the actual moisture transport rates in concrete (see Ref. [13]), and to deduce thereby the material behaviour in natural environments.

4. Water vapour desorption and adsorption isotherms: link between pore structure and moisture properties

4.1. Effect of the presence of aggregates and of the specimen size: comparison hcp/concrete

The WVSIs obtained at $T=23\pm0.1$ °C from the experiments described in Section 3 on hcp C (crushed specimens) and concrete B (slices), mixed with same cement (series 1) and with W/C = 0.45, are compared in Fig. 1a. The plots are the mean values calculated from at least three specimens. Note that a very good repeatability was observed on the measurements. In order to allow a direct comparison between the results obtained on concrete and hcp, the water contents are expressed here in percentage per unit mass of ''dry'' (*i.e.* at ''equilibrium'' state at RH = 3%) hcp contained in the material. Very similar isotherms are obtained for the hcp and the concrete over the whole RH

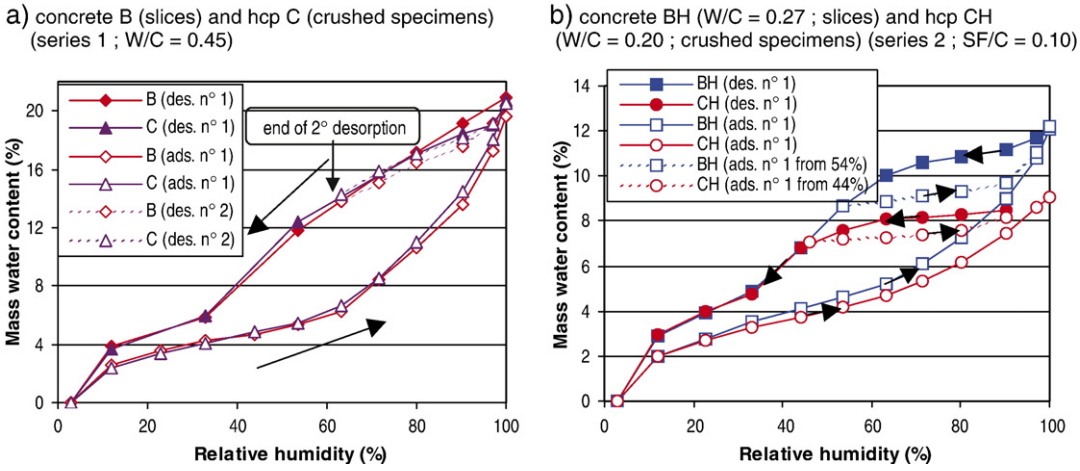

Fig. 1. Water vapour desorption and adsorption isotherms measured at $T=23\pm0.1$°C on concretes and hcps, after sealed curing. The water contents are expressed in percentage per unit mass of "dry" hcp contained in the material. The "temporary" end of the sorption experiments is marked.

range. It can be concluded that the presence of aggregates does not influence the WVSIs of hardened materials. This can be explained by the fact that the void size range, where the moisture equilibrium processes described by the isotherms take place, is much smaller than the paste-aggregate interface heterogeneities and the typical voids present in this zone. Concrete and hcp textures, in the micro- and the meso-pore ranges investigated by water vapour sorption processes, are therefore identical (bulk cement paste pore structure).

Likewise, Fig. 1b shows that, for RH ≤44%, the WVSIs of the hcp CH (crushed specimens) and concrete BH (slices) match perfectly. Therefore, within this RH range, the same conclusion (as that from Fig. 1a) can be drawn, with respect to these HP materials mixed with same constituents but with different W/C (series 2): the presence of aggregates does not influence WVSIs. Moreover, Fig. 1b reveals the range of influence of W/C, which will be studied in details in Section 4.4.

Furthermore, Fig. 1 highlights that specimen size, as well as calibrated and moderate crushing (3-mm thick slices compared to 1-mm crushed specimens), don′t influence the results.

4.2. Hysteretic behaviour

The WVSIs obtained at $T=23\pm0.1$ °C on normal hardened concrete B (slices) and hcp C (crushed specimens) from series 1, on normal hardened concrete BO (slices) and hcp CO (crushed specimens) from series 2, and on HP hardened concrete BH (slices) and hcp CH (crushed specimens) from series 2, are displayed in Fig. 2. Each plot of the curves is the average of experimental values obtained on at least two specimens. In addition to the 3–100% first adsorption isotherm, first adsorption curves, which start from various RHs (RH=12%, 33%, 44%, 53.5%, 63.2% or 71.5%, depending on the material), are also plotted in Fig. 2 (scanning isotherms). For some materials, the beginning of the second adsorption isotherm from RH=3% is also displayed. Likewise, second (or third) desorption curves, which start from RH=100%, 97% or 90.4% after various hygral paths (*i.e.* desorption–adsorption sequences), are presented. In particular, cycles performed within the RH range [44% ; 100%] are shown.

The results exhibit an hysteresis between desorption and adsorption, extending over the whole RH range, whatever the mixture. This hysteresis is more significant within the mid-range. Within this range, the capillary condensation and evaporation, according to the well-known *Kelvin* equation with the assumption of constant gas pressure (equal to the atmospheric pressure), is assumed to be the mechanism which governs the thermodynamic equilibrium between water in liquid and gaseous phases in a pore. Therefore, the Van der Waals loop of a confined fluid, whose shape is affected in particular by the degree of constriction of the pores [22], the ‘‘inkbottle effect’’, as well as the possible different liquid-vapour interface shapes (curvatures) and more roughly speaking a different pore filling between desorption and adsorption, are usually assumed to explain the hysteresis observed within this range with various fluids and various porous materials. Within the low RH range (in particular when RH ≤ 33%), the hysteresis between first desorption and adsorption is drastically reduced (see Fig. 2), as a result of the reduction of the previously mentioned phenomena. According to Feldmann [24], irreversible phenomena linked to the removal of interlayer water (*i.e.* strongly bound to the C–S–H, see Section 4.4), which induce simultaneous collapse of the pore structure (in particular for RH=10–20% [53]), can explain the hysteretic behaviour observed within this low RH range and observed only in the case of water. As a matter of fact, no hysteresis occurs within this low RH range with inert gas such as nitrogen (see for example the nitrogen adsorption–desorption isotherms measured after vacuum outgassing by Baroghel–Bouny with the hcps C, CO and CH in [33], or the data published in [49]). The described phenomena are usually assumed to yield irreversible shrinkage and change in the C–S–H ‘‘gel’’ structure. Note that here the hysteresis between first desorption and adsorption is particularly reduced within the low RH range, as the drying of the specimens is mild (desorption at RH=3% and at $T=23\pm0.1$ °C, see Section 3.4). The hysteresis between first desorption and adsorption can be further reduced by a moderate increase in the test temperature (see later). Note in addition that the uptake of molecules through pore openings of about the same width as that of the adsorbate molecules (see Section 4.4) is likely to induce irreversibility [40]. The multiple-sized inkbottle pores, involved in the model proposed by Jennings et al. [53,57], can also explain the hysteresis recorded within the whole RH range on the WVSIs (and on length change and modulus), as well as the differences recorded between nitrogen and water sorption data. Furthermore, it is worth reminding that kinetic effects, which complicate and delay the establishment of equilibrium, can also contribute to enhance the hysteresis [33] over the whole RH range and more particularly in the mid-range where moisture transport is the slowest according to [29,33,54–56] (see Section 3.5).

As expected, the initial point and the hygral path (*i.e.* moisture history) influences the (residual) ‘‘equilibrium’’ water content recorded. Nevertheless, Fig. 2 shows that for every material, the various first adsorption curves to 100%, whatever their starting point, reach the first 3%–100% adsorption isotherm. In addition, after the second desorption, the first desorption mass at RH=3% seems to be restored (at least for the few data already available) and the second adsorption isotherm from RH=3% overlays the first one (see e.g. Fig. 2a and e). The first 3%–100% adsorption isotherm can thus be regarded as the ‘‘boundary’’ adsorption isotherm. Note that irreversibility in the mass in the dry state can be recorded when stronger drying is carried out [26]. Moreover, for every material, the second (or third) desorption isotherm from RH=100% overlays the first 100%–3% desorption one (‘‘boundary’’ desorption isotherm), at least above RH=44%. Below this RH, the second desorption curve is shifted upwards, compared to the first one, for normal materials, revealing an enhanced hysteresis when the second adsorption isotherm from RH=3% is available. When starting below RH=100% (*i.e.* here at RH=97% or 90.4%), the second desorption curves remain under the ‘‘boundary’’ desorption isotherm and reach it at about 44%. The saturation state of the

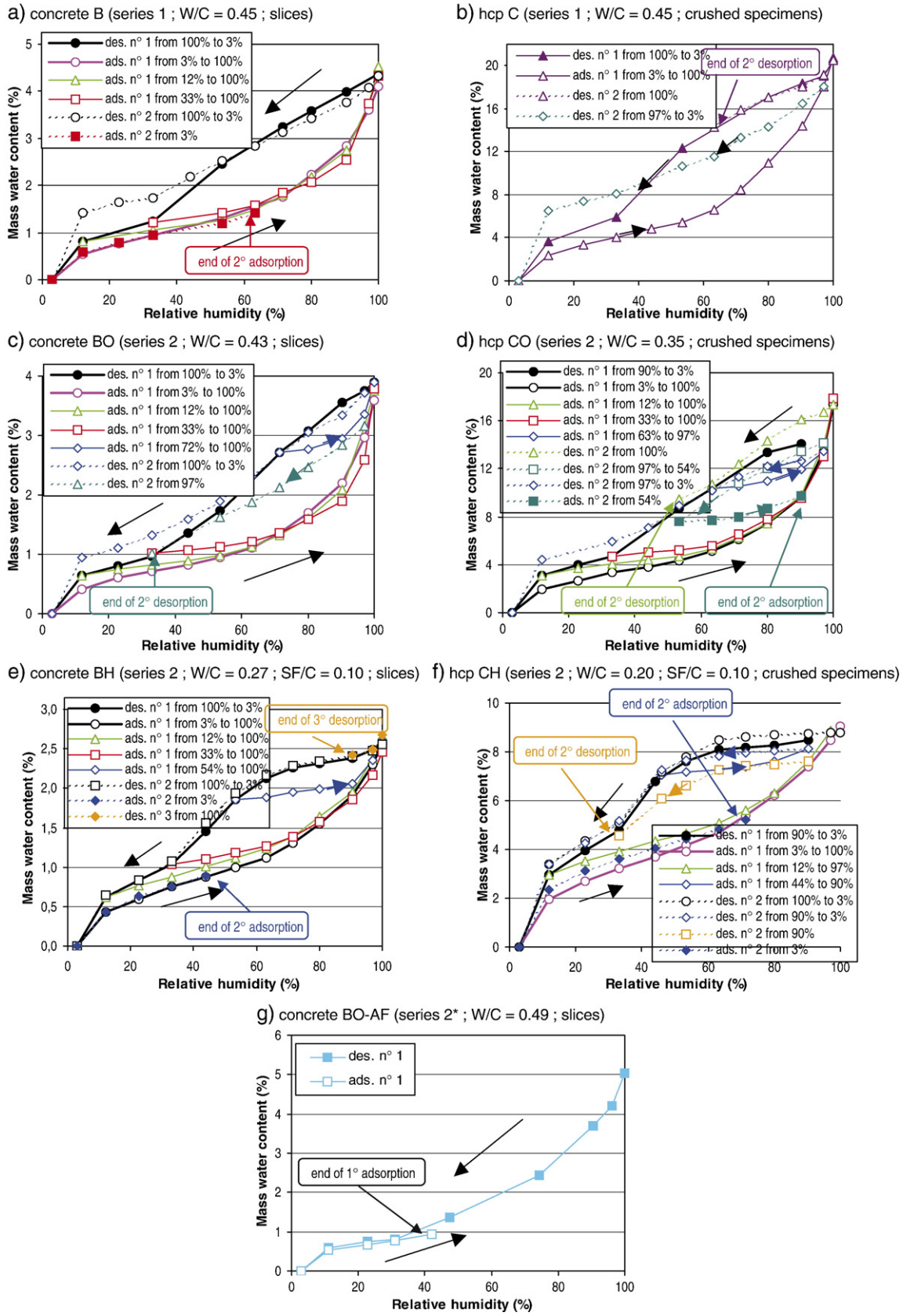

Fig. 2. Water vapour desorption and adsorption isotherms and scanning isotherms within various RH ranges, measured at $T = 23 \pm 0.1$ °C on various concretes and hcps after sealed curing, and at $T = 44 \pm 0.1$ °C on concrete BO-AF after wet curing. The "temporary" end of the sorption experiments is marked.

pore system (*i.e.* the pore filling with the liquid phase) at the starting point is indeed not as complete as in the initial state and the desorption is thus likely to be different within the whole capillary range. Therefore, cycles (scanning loops) performed within the ''equilibrium'' RH range [44% ; 100%] (*i.e.* within the capillary range, see Section 4.4.3) remain inside the area delimited by the ''boundary'' desorption and adsorption isotherms. The existence of such ''boundary'' isotherms is therefore of great practical interest. After a whole desorption–adsorption process, the initial water content at RH = 100% seems to be restored, even if the difficulties to assess an ''equilibrium'' state at this RH by the method used here induce some variability in the mass recorded. This means that the overall pore volume is not changed. The difficulties result from the high sensitivity of the process to temperature at this RH, which induces non-stable condensation–desorption phenomena, and from the occurrence of macro-condensation. The range 95–100% is indeed often regarded as a transition zone between the hygroscopic and over-hygroscopic ranges. As a matter of fact, above RH = 99%, water movements in ''big'' pores are involved ($r_p > 10^2$ nm, according to Kelvin equation). More generally, whatever the path and the RH range, when a complete cycle (loop) has been performed, the initial point on the ''boundary'' isotherm is rejoined (see for example the 100%–33%, 100%–71.5%, 97%–63.2%, 100%–12%, and 90.4%–44% loops in Fig. 2a, c, d, e, and f, respectively). These results are in accordance with those published earlier by Feldman [24].

The WVSIs obtained at $T = 44 \pm 0.1$ °C on normal concrete BO-AF (slices) are displayed in Fig. 2g (mean values calculated with at least two specimens). The available data (first desorption and beginning of first adsorption isotherms) do not exhibit any hysteresis in the low RH range. According to the literature [20,26,81], a temperature rise, such as from $T = 23 \pm 0.1$ °C to $T = 44 \pm 0.1$ °C, induces a slight shift towards the lower water contents of both the desorption and adsorption isotherms over a broad RH range (more significantly for the desorption isotherm). Analytical formula have been proposed to describe this effect (as a result of the temperature dependency of the surface tension, the density of liquid water and the saturating vapour pressure). However, pure thermodynamic temperature effects are not sufficient to explain the coincidence between desorption and adsorption curves displayed in Fig. 2g. Another affect has to be regarded: from a thermodynamic point of view, the inkbottle effect is a ''metastable'' state. This means that hysteresis is likely to be reduced after a long period of time (which will depend on the RH range and on the test temperature), and will tend to vanish after an ''infinite'' period of time. Since a temperature rise drastically increases the rate of water vapour and dry air diffusion, as well as of Darcean liquid transport, and hence of desorption, it will favour dissipation of inkbottle effect and obtaining thermodynamic equilibrium. This yields a desorption isotherm closer to the adsorption one (which is slightly affected by temperature). Data at $T = 23 \pm 0.1$ °C on exactly the same material are not available, but a comparison of the BO-AF results with those obtained at $T = 23 \pm 0.1$ °C with other materials with W/C in the same range (see Sections 4.3 and 4.4) confirms that the coincidence of the desorption and adsorption curves probably results from a more significant shift towards the lower water contents of the desorption curve when the temperature increases. Of course more data are needed to confirm this aspect, and the exposure time required for the hysteresis to disappear within the whole RH range is not accessible for practical applications. Nevertheless, this analysis points out the importance of kinetics effects and reveals the hysteresis as a ''short-term'' phenomenon. This tends to confirm the nature and the reversible feature of the processes (e.g. inkbottle effect).

Differences between first and second desorption isotherms have already been reported in the literature and are attributed in particular to a significant instability of the pore structure during the first desorption [24,53,55,56,58]. For example, Feldmann [24] recorded a coarsening of the pore structure. According to Jennings et al. [53,57,58], drying causes re-structuration of low density (LD) C–S–H and more precisely their collapse below RH = 40%, as well as conversion of loose-packed (LP) C–S–H to LD C–S–H. The authors explain, on the basis of a colloidal description of the C–S–H (see also Scherer [59]), that drying enhances the chemical ageing, which means the C–S–H particle bonding over time, increasing the degree of polymerization of the silicate chains and changing ''irreversibly'' the C–S–H in stiffer, stronger and denser ones. The second and subsequent desorptions are usually found similar. Thus, the pore structure obtained after first desorption is usually considered as more stable and the second desorption more representative of this pore structure [56]. In addition, the second desorption curve can be preferred within the high RH range, as it is less affected by self-desiccation, etc.

The experimental results obtained here confirm the microstructural changes. More precisely, the higher water contents measured during the second desorption in the low RH range (in particular between 33% and 12%) indicate that a collapse took place during the first desorption, and that the resulting water amounts retained in the material after adsorption and second desorption (enclosed in the compressed C–S–H ''gel'') were not able to be removed unless re-exposure to RH = 3% (*i.e.* when pores with very small openings could be desorbed). In a way, the first desorption to RH = 3% (and its associated ''irreversible'' shrinkage) has extended the inkbottle effect to the low RH range (compare the different shape and magnitude between first and second hysteresis loops in Fig. 2). However, the difference between first and second desorption isotherms depends greatly on the material. The negligible difference observed even within the range RH ≤ 44% in the case of BH and CH (see Fig. 2e and f, respectively) can be explained by the fact that these materials contain a very small capillary pore volume and a very small amount of LP/LD C–S–H (they are mainly constituted of HD, *i.e.* high-density, C–S–H, see Section 4.4).

However, it seems that the changes recorded here at room temperature and on mature materials, are only temporary, rather than ''permanently'' irreversible, changes, as illustrated in particular by the restoration of the first desorption mass at RH = 3% and by the fact that the second adsorption isotherm from RH = 3% overlays the first one. This conclusion with respect to the

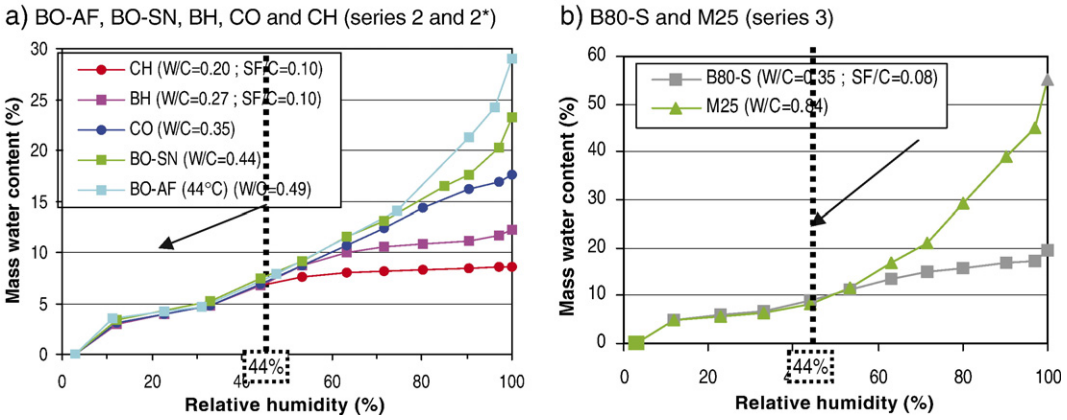

Fig. 3. Comparison between water vapour desorption isotherms of normal and HP materials, measured at $T=23\pm0.1$ °C and at $T=44\pm0.1$ °C (BO-AF). The water contents are expressed in percentage per unit mass of "dry" hcp contained in the material.

reversibility is of primary importance for the understanding of the mechanisms and the modelling of moisture transport, drying shrinkage or creep. Furthermore, all of this confirms the validity and the repeatability of the measurements and their "intrinsic" feature, as already pointed out by previous data obtained by the author [33]. These results show *a posteriori* that neither continued progress of the hydration reactions nor chemical alteration (e.g. carbonation) affected in a significant manner the equilibrium properties of the material during the test, in spite of its long duration (several years).

4.3. Comparison between normal and HP materials

Since various grades of normal concretes (from the porous M25 to the dense BO), as well as HPCs (BH and B80-S) are tested here, the moisture properties of these various materials can be compared, in particular that of the normal and HP concretes.

The water vapour desorption isotherms (WVDIs) obtained with the normal (BO-AF, BO-SN and CO) and HP (BH and CH) hcps and hardened concretes from series 2 and 2* are compared in Fig. 3a. Likewise, the WVDIs obtained with the low-grade concrete M25 and the HPC B80-S from series 3 are compared in Fig. 3b. Here again, the isotherms are identical at least for RH ≤ 44%. But a large difference is recorded between normal and HP materials above this range. Note that the difference recorded when the measurements are performed at $T=44\pm0.1$ °C is not very significant (see Section 4.2). Figs. 1b and 3 exhibit the peculiarities of HP materials as regards their moisture properties within the high RH range. Significant lower water contents are measured for HP materials than for normal materials. Moreover, large RH variations induce only slight changes in water content for HP materials (see for example in Fig. 1b the scanning isotherms carried out within this range, and also [31]). This is the result of a low W/C and of incorporation of SF, and will be discussed in more details in Section 4.4. Furthermore, if the WVDIs are plotted as $S_l=S_l(RH)$, where S_l is the degree of liquid water saturation, it becomes obvious that, at a given RH, a significantly larger portion of the pore volume of the HPCs (see BH and B80-S in Fig. 4), compared to that of normal concretes, is filled with the liquid phase (see also Section 5). In Fig. 4, $S_l<1$ at RH = 100%, since the bulk porosity accessible to water measured by hydrostatic weighing [60], and which is slightly larger than that deduced from WVDIs for the considered concretes (see Section 4.4.5), has been taken into account in the computation of S_l.

All of this indicates that HP materials will be weakly sensitive to environmental RH changes (weathering variations) within a broad range (see Section 5). In particular, it can be deduced from the WVSIs that HPCs will display reduced moisture losses and deformations associated with external drying at RH ≥ 50% [61]. This will influence the durability-related properties of these materials. In addition, these results are particularly useful for explaining the behaviour of structures submitted to daily and season fluctuations in natural environments, where the average conditions are most of the time within this range.

4.4. Analysis of desorption and adsorption isotherms and relation to pore structure

4.4.1. Relevance of the analysis

In the course of water vapour desorption–adsorption processes, hardened cementitious materials undergo simultaneous

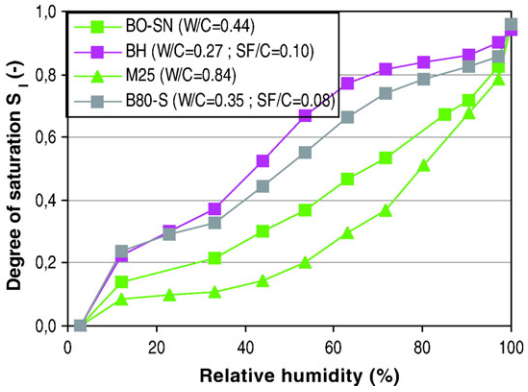

Fig. 4. Comparison between water vapour first desorption isotherms, plotted as S_l *vs.* RH, of normal and HP concretes (series 2, 2* and 3), measured at $T=23\pm0.1$ °C.

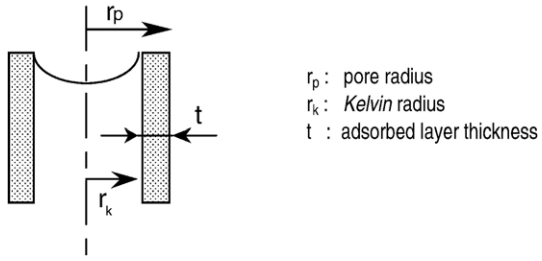

Fig. 5. BJH model: co-existence of ‘‘capillary’’ and ‘‘adsorbed’’ phases in cylindrical pores.

volume changes likely to affect a pore structure analysis performed from WVSIs and to yield a misleading description. Nevertheless, the relation of water to cement-based-material behaviour and durability, along with the origin itself of the porosity of these materials, make the water molecule the ideal probe for the investigation of their pore structure in relation to actual macroscopic behaviour. In addition, a comparative investigation between for example different mixtures will remain valid in any case and particularly useful. Therefore, a pore structure analysis has been performed here from the experimental WVSIs discussed in this paper.

4.4.2. Pore size distribution in the mesopore range (BJH calculation)

The BJH method proposed by Barrett, Joyner and Halenda in 1951 [62] allows the determination of the pore size distribution in the mesopore range (pore openings between 2 and 50 nm, according to IUPAC classification [40]) and in the micropore range (openings <2 nm [40]) investigated by sorption isotherms. The main assumption of this method is the co-existence of ‘‘capillary’’ and ‘‘adsorbed’’ (water) phases in cylindrical pores (see Fig. 5). The iterative computation is based on the step-by-step analysis of the desorption curve. Desorption at a given RH corresponds to (see Fig. 5) [40,62]:

- removal of water condensed in pores, whose radius r_p(RH) takes into account the capillary pore space governed by Kelvin equation (Kelvin radius r_k) and the adsorbed multimolecular water layer (thickness t, see Section 4.4.4),
- decrease of the adsorbed water layer thickness, in pores with radius $> r_p$.

Owing to greater experimental difficulties, this method has been less often used with water vapour (at room temperature) than with nitrogen gas (at $T = 77$ K). The BJH model can appear far from the actual microstructure of cementitious materials, in particular when compared to the sophisticated models currently developed to describe this microstructure. Nevertheless, the BJH method remains relevant and useful at least for comparative studies. In addition, it is worth noting that in a recent paper, Coasne et al. [22] highlighted a rather good agreement between their model and the BET method (see Section 4.4.4) in the case of a pore with constriction. As regards the BJH method, they found that the geometrical pore size is underestimated in particular when the pore size decreases, but that the main features are kept.

The BJH method has been applied here with the ‘‘t curve’’ proposed by Hagymassy et al. in [63] (see Section 4.4.4). Examples of pore size distributions then obtained on hcps C, CO and CH, and on concretes B, BO and BH, are displayed in Fig. 6 [32,33,64]. The graphs exhibit a main pore mode, the maximum of which is located identically for all the mixtures at $r_p \approx 1.7$ nm. This value is in agreement with the results obtained with nitrogen by automatic apparatus at $T = 77$ K on hcps C, CO and CH ($r_p \approx 1.7$ nm, see Fig. 7), and is not very different from those obtained by thermoporometry (DSC) on hcp C ($r_p \approx 2.2$ nm, see [33]). This result is also in agreement with the literature, where a pore mode located at $r_p = 1.8$ nm is usually described. In addition, it is observed that the bulk C–S–H ‘‘gel’’ pore volume is associated with $r_p \leq 5$ nm (*i.e.* RH ≤ 76%, according to BJH calculation).

The peculiarities of HP materials, highlighted in Section 4.3 as regards moisture properties, reflect their peculiarities as regards the pore network. The WVSIs of these materials (as well as the MIP results [65]) depict a very fine pore network: as a result of a low W/C and the use of SF, a very small pore volume

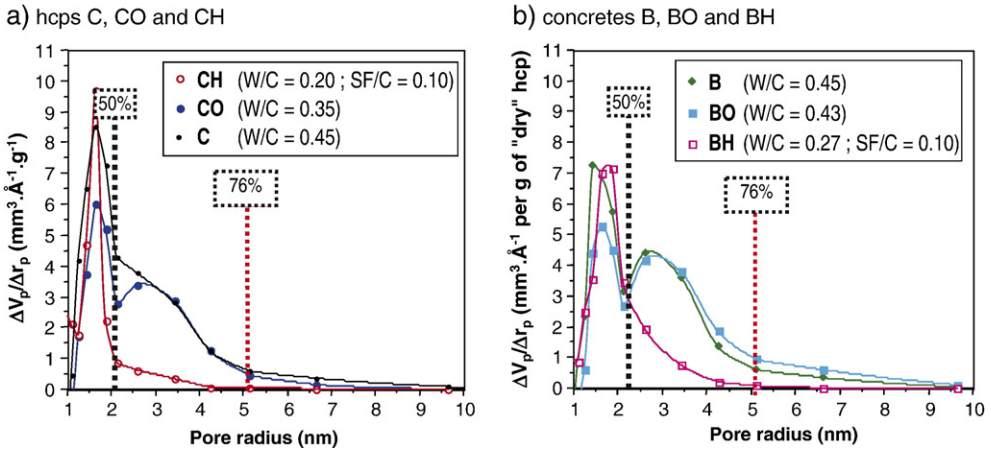

Fig. 6. Pore size distributions in the mesopore range (BJH calculations) from water vapour sorption isotherms measured at $T = 23 \pm 0.1$ °C.

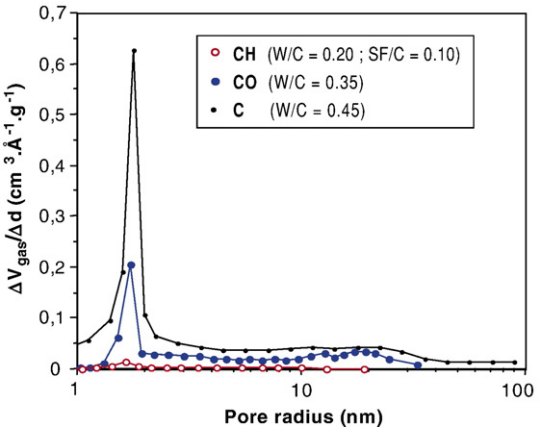

Fig. 7. Pore size distributions in the mesopore range (BJH calculations) from nitrogen sorption isotherms measured on hcps C, CO and CH by automatic apparatus at $T=77$ K (age=1.5 year), after vacuum outgassing.

is associated with $r_p \geq 2$ nm (see Fig. 6), which corresponds with RH ≥ 50% according to BJH calculation, and which means in particular a very small capillary porosity. More precisely, the significant pore volume displayed for normal materials within the range $2 \leq r_p \leq 5$ nm (maximum located around 3 nm) is lacking in the pore size distribution of HP materials. Therefore, a very small pore volume is involved in the wetting–drying processes above RH=50%, likely to occur in various natural environments.

Similar results are found for concretes and hcps (see Fig. 6). This confirms that BJH calculations from WVSIs allow an accurate description of the nanostructure (e.g. C–S–H ''gel'' pore structure) from hcp as well as concrete specimens, and can for example complement MIP data [66]. This point is of importance, since it is more often concrete mixtures that one needs to characterize than hcps, but very few physical or chemical techniques allow a direct analysis of concrete specimens.

As far as cementitious materials are concerned, water is hardly replaceable by other molecules. Nitrogen, argon or oxygen could be easier to use and provide useful data (see e.g. [48]), but are not suitable to characterize the entire pore structure of these materials. As a matter of fact, the measurements carried out with nitrogen on hcps C, CO and CH provide a pore volume that drastically decreases with W/C within the range $1 \leq r_p \leq 2$ nm (see Fig. 7). In particular, the volume measured with the high-performance CH is very small. This ''irrelevant'' finding (see Section 4.4.6), as well as an underestimated specific surface area [33] (see Section 4.4.4), are the result of at least the bigger size and the lower affinity for the cement matrix of nitrogen molecules than water molecules, and certainly of inappropriate drying and outgassing, which do reduce the accessibility to the entire pore system in particular in

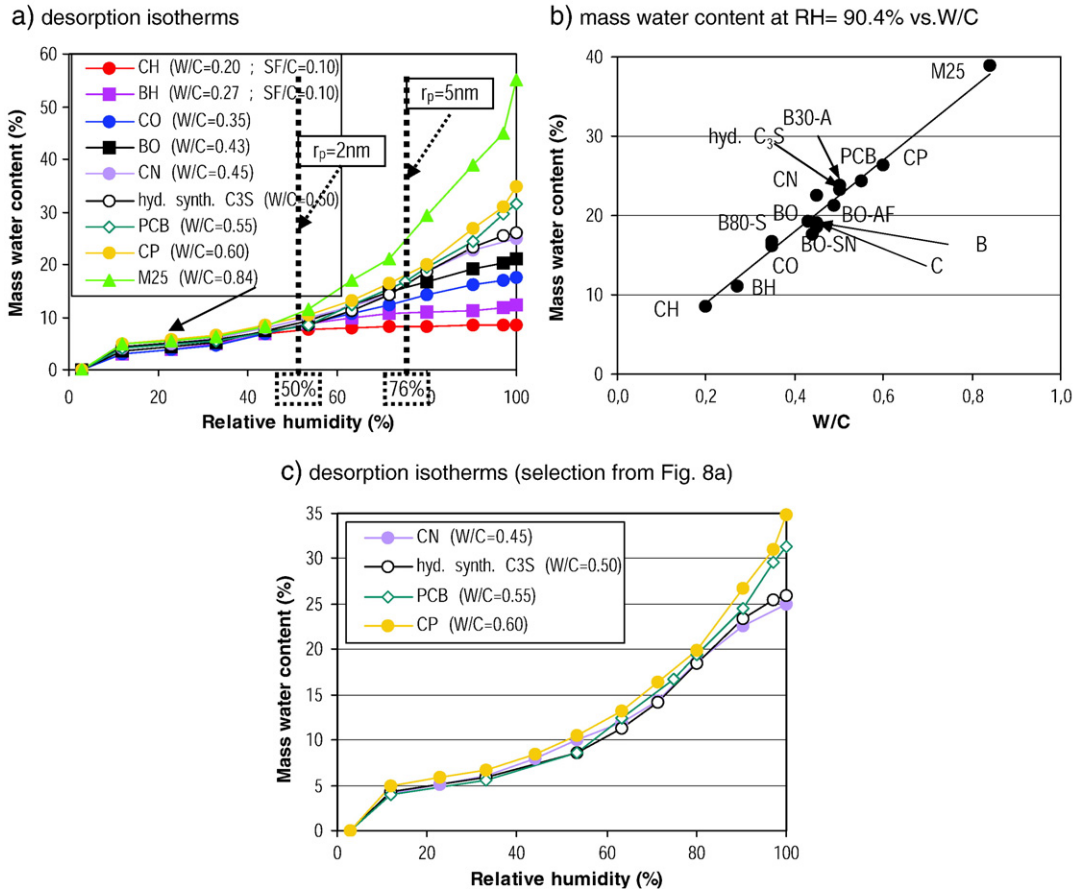

Fig. 8. Water vapour desorption isotherms measured at $T=23 \pm 0.1$ °C on various materials, and correlation between ''equilibrium'' mass water contents at RH=90.4% and W/C for all the tested materials. The water contents are expressed in percentage per unit mass of ''dry'' hcp contained in the material.

the case of dense HP pastes [33,48,52,53,67]. The difference in thermal energy of adsorption between the two types of experiments can also significantly influence the results.

4.4.3. Effect of mix-parameters on desorption isotherms

The effect of mix-parameters and in particular of W/C on the ''equilibrium'' moisture properties can be deduced from the WVDIs displayed in Fig. 8a and obtained on various hcps and concretes. A relevant partition of the isotherms is highlighted, identifying several RH ranges regardless of the material, where the ''equilibrium'' water contents are affected or not by W/C (or other mix-parameters). These RH ranges are based on the BJH pore size distributions given in Fig. 6 and on the pore system description proposed by the author in [33]:

●*For RH>76%*: prominent influence of W/C (''pure'' capillary range: $r_p \geq 5$ nm)

When W/C decreases, the capillary porosity is reduced and the pore network becomes finer ; the less porous the material, the lower the ''equilibrium'' water contents. This is mainly W/C which determines the ''equilibrium'' desorption water contents within the high RH range (wide spreading of the curves). As a matter of fact, a linear relationship is pointed out between ''equilibrium'' first desorption water contents at RH=90.4% and W/C (see Fig. 8b) for the various hcps and concretes tested, whatever the cement, the test temperature, the age and the curing conditions,

●*For 50%≤RH≤76%*: mitigated influence of W/C and other mix-parameters (SF)

No linear relationship with W/C can be exhibited. WVDIs are still influenced by W/C, but this effect is reduced and is no more the single one (see also [33]). This can be explained by the fact that within this range water from the pores between the C–S–H ''gel'' clusters ($2 \leq r_p \leq 5$ nm, according to BJH calculations, see Section 4.4.2), more precisely between outer C–S–H products (or between LD C–S–H, according to the model from Jennings et al. [53,57,58]), is removed by the desorption process [33,64,65]. The difference recorded between the various WVDIs as a function of the mix-composition seems in accordance with the characteristics of the C–S–H, in particular the relative proportion of LD C–S–H, in the material. For example, the flat WVDI and the very small pore volume recorded within this range with CH denote a very small amount of LD products. This finding is in agreement with the C/S results [36] and the morphological features [33,65] revealed by microscope investigations and reported in previous papers by the author (see also [68]). In CH, the C–S–H are mainly dense, amorphous and featureless products (*i.e.* type III and IV or HD C–S–H, depending on the terminology/model used). When observed by BSE-SEM, CH appears as a two-phase ''homogeneous'' material, which is composed of unreacted cement grains and dense C–S–H [33]. No distinction can be made in this case between inner and outer products. Conversely, outer C–S–H products, which are fibrous, rather well developed (type I) and reticulated or honeycomb ones (type II), are easily observed in normal materials. This is also quite consistent with the model proposed by Jennings et al., which states that 50% of the products are LD C–S–H and 50% are HD C–S–H in mature materials with W/C around 0.40, and that more LD C–S–H form at higher W/C [53,57,58]. Note that the same W/C threshold has been pointed out in [36], with respect to various microstructural characteristics (in particular that of the C–S–H) and macroscopic properties. Such a peculiarity of HP materials like CH can be attributed to the small space (as a result of the initial spacing between particles) and amount of water available, and maybe to the specific chemical composition of the liquid phase induced by the presence of silica fume,

●*For RH<50%*: almost no influence of W/C (except in the case of very high W/C) or other mix-parameters

The WVDIs are very similar for all the materials tested. This finding illustrates that, within this range, moisture equilibrium takes place in a pore structure (r_p <2 nm, according to BJH calculations, see Section 4.4.2) not affected by mix-parameters: the pores internal to the C–S–H ''gel'' clusters (more

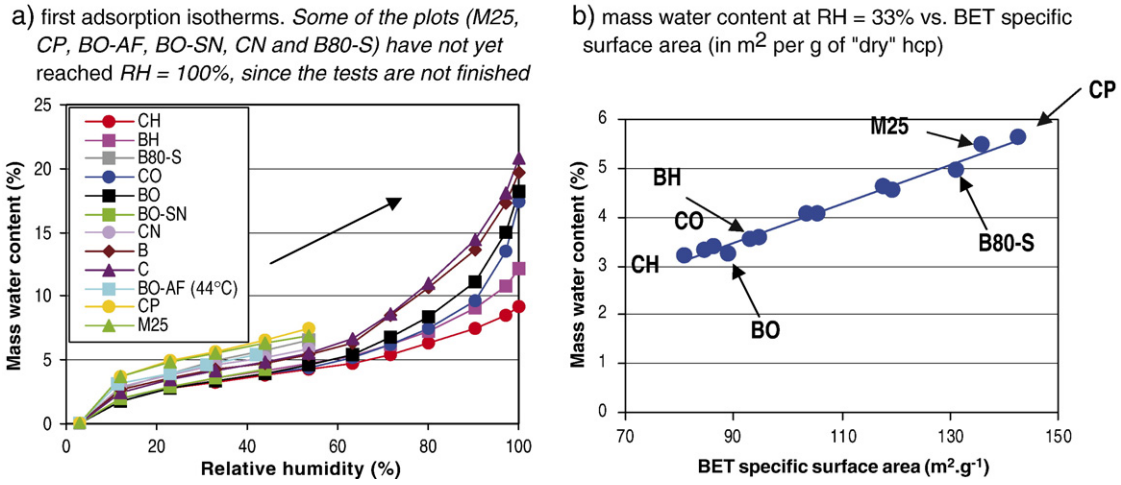

Fig. 9. Water vapour first adsorption isotherms measured at $T=23\pm0.1$ °C and at $T=44\pm0.1$ °C (BO-AF) on various hcps and concretes (series 1, 2, 2* and 3; $0.20 \leq W/C \leq 0.84$; $0 \leq SF/C \leq 0.10$), and correlation between ''equilibrium'' mass water contents at RH=33% and BET specific surface area accessible to water molecules. The water contents are expressed in percentage per unit mass of ''dry'' hcp contained in the material.

particularly the inner and HD C–S–H). The very slight shift observed as a function of the mix-composition can be attributed to the different C–S–H amounts (see Fig. 12b in Section 4.4.4). In particular, the highest water contents are obtained for the materials which display the highest C–S–H amounts, as a result of a very high W/C (CP, M25), or of a medium–low W/C with SF (B80-S). The smallest pores (so-called intra-crystallite pores, interlayer pores or nanopores internal to C–S–H globules) are also involved within this range, more exactly below RH = 22.8%.

Figs. 3a, b, 8a and c (Fig. 8c is a selection from Fig. 8a, which includes only the hcps CP, CN, PCB and the hydrated synthesised C_3S) illustrate how similar can be the WVDIs, in particular within the range RH ≤ 44%, whatever the cement (even in the case of plain C_3S) and the casting process. This highlights the same arrangement of the C–S–H ''gel'' clusters and confirms the high degree of repeatability of the measurements.

4.4.4. Analysis of adsorption isotherms — assessment of specific surface area, C–S–H ''gel'' amount and adsorbed water layer thickness

A similar type of analysis as in the previous section can be performed with the adsorption isotherms displayed in Fig. 9a (various hcps and concretes from series 1, 2, 2* and 3 with 4 OPCs CEM I — 52.5 ; W/C ranging from 0.20 to 0.84 ; SF/C ranging from 0 to 0.10). Note that the experimental values lie within the same range as that of the data recently published on hcps in [26] (W/C = 0.35, 0.45 and 0.50) or in [27] (W/C = 0.30, 0.40 and 0.50). A linear variation as a function of RH is observed within the low RH range, from RH = 12%.

4.4.4.1. Specific surface area. The determining influence of the specific surface area on the adsorption isotherms is pointed out within the low RH range (see Fig. 9b). Here, the specific surface area accessible to water molecules (S_{sBET}) of the hcps and concretes tested has been calculated within the low RH range of the experimental water vapour adsorption isotherms (WVAIs) by the BET method proposed by Brunauer, Emmett and Teller in 1938 [18], which assumes that the fluid covers uniformly the pore walls (see also [33,40,66]). The S_{sBET} values range from 80 for CH (degree of hydration $\alpha = 0.48$, see Table 2, and SF/C = 0.10) to 143 $m^2\ g^{-1}$ for CP ($\alpha = 0.92$). Note that for concretes, the values are given in m^2 per g of ''dry'' hcp contained in the material.

The orders of magnitude of the experimental results found here are in agreement with the literature: for a fully hydrated cement paste, S_{sBET}(water vapour adsorption) values between 100 and 200 $m^2\ g^{-1}$ have been reported [21,23,24,67,69–71]. The results published as regards proton nuclear magnetic resonance (^{1}H NMR) seem also in agreement [52,72]. Note in addition that, more generally, specific surface areas (measured by N_2 adsorption, MIP, small-angle X-ray or neutron scattering SAXS-SANS, or NMR) range between 80 and 300 $m^2\ g^{-1}$, according to [52]. It can also be deduced from the literature that the ratio S_s(SAXS-SANS)/S_{sBET}(water vapour adsorption) is around 1.5 [52,73,74].

The C–S–H ''gel'' amount, which is a function of the binder content, the degree of hydration of the cement (hydraulic reaction) (and hence the W/C) and the pozzolanic reaction, determines the specific surface area (see Fig. 10 and [64] or [66]). In particular, authors have published data exhibiting a linear relationship between specific surface area and degree of hydration for plain cementitious materials (see e.g. Ref. [72] in the case of NMR-based specific surface area, and see also Fig. 10b). Therefore, similar BET specific surface areas are found for CO (resp. BO) and CH (resp. BH) with silica fume, despite a lower W/C (*i.e.* degree of hydration) for CH (resp. BH), as illustrated in Figs. 9b and 10. Likewise, similar and high BET specific surface areas are found for CP and M25 (high W/C) and B80-S (high binder content, medium–low W/C with silica fume) (see Figs. 9b and 10). From Fig. 10b, it is possible to deduce for a hcp like CH its ''equivalent'' degree of hydration (*i.e.* the degree of hydration of a SF-free hcp with same specific surface area and thus same C–S–H ''gel'' amount): $\alpha = 0.73$. The same type of calculation can be carried out for BH and B80-S ($\alpha = 0.77$ and $\alpha = 0.88$, respectively). It can be deduced from all of this that

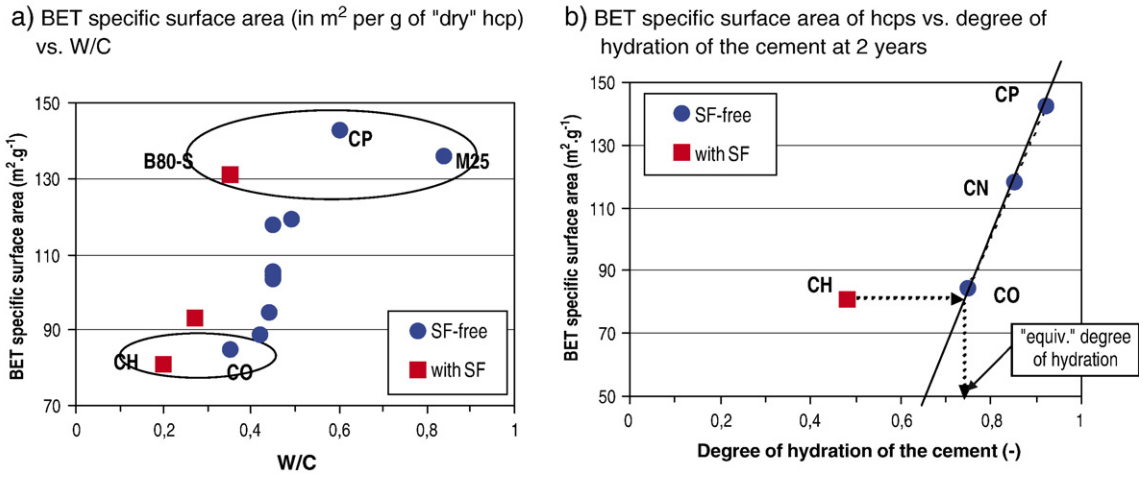

Fig. 10. Correlation between BET specific surface area accessible to water molecules and W/C or degree of hydration of the cement (average value between BSE-SEM image analysis and thermogravimetric analysis).

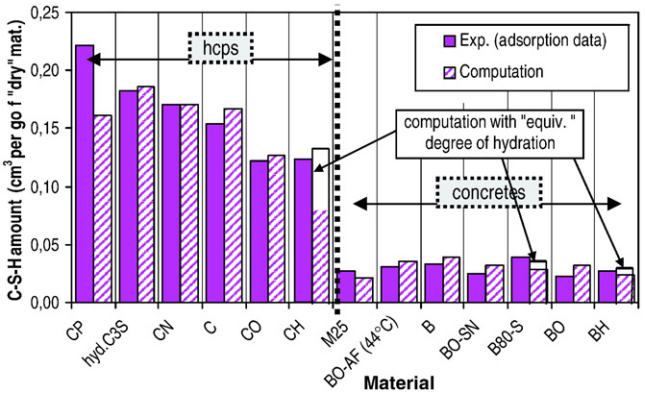

Fig. 11. C–S–H ''gel'' amounts deduced from the experimental water vapour adsorption isotherms measured on hydrated synthesised C_3S, hcps and concretes (series 1, 2, 2* and 3; $0.20 \le W/C \le 0.84$; $0 \le SF/C \le 0.10$). Comparison with the amounts computed by means of an analytical hydration model.

the ''equilibrium'' water amounts adsorbed (at least within the range RH ≤ 44%) will be also linearly related to the C–S–H ''gel'' amount, as it will be illustrated later. This explains the differences between the various materials displayed in Fig. 9a.

4.4.4.2. Assessment of C–S–H ''gel'' amount. It is difficult to measure directly the C–S–H ''gel'' amount by usual chemical techniques, owing to the low crystallinity and the variable composition (stoichiometry) of the C–S–H. In addition, the computation of this amount by means of hydration models is not easy when the material contains supplementary cementing materials. Yet, its determination is required in numerous cases, such as modelling of carbonation or of chloride binding in concrete [3,75].

It can be deduced from the observations previously mentioned that this amount can be assessed through adsorption data, by using a method similar to that described by Olson and Jennings in [76]. The C–S–H ''gel'' amount, expressed in cm^3 per g of ''dry'' hardened material, is calculated here as the ratio of the water amount adsorbed by the material at RH = 22.8% (in g per g of ''dry'' material) to the water amount adsorbed by the C–S–H at RH = 22.8% (in g per cm^3 of C–S–H). The water amount adsorbed by each tested material at RH = 22.8% is directly provided by its WVAI. As far as the water amount adsorbed by the C–S–H is concerned, it can be directly assessed from experiments on the fully hydrated synthesised C_3S. As explained in [76], this is the ratio of the water amount adsorbed by this material at RH = 22.8% (in g per g of ''dry'' material) provided by its WVAI to the C–S–H amount (in cm^3 per g of ''dry'' material) deduced from the $Ca(OH)_2$ and free water amounts measured by thermogravimetric analysis (as this material does not contain any other compound). The water amount adsorbed by the C–S–H at RH = 22.8% thus obtained is 0.219 g per cm^3 of C–S–H (by using 2.6 g cm^{-3} for the C–S–H density in this state, according to [76]). The value determined by *Olson and Jennings* in [76] at RH = 20% on D-dried C_3S pastes was 0.26 g per cm^3 of $C_{3.4}S_2H_3$.

The C–S–H ''gel'' amounts (in cm^3 per g of ''dry'' material, *i.e.* at ''equilibrium'' state at RH = 3%) obtained here experimentally have been compared in Fig. 11 to the C–S–H amounts provided from the mix-composition, the mineralogical composition of the cement and its hydration kinetics, by using an analytical hydration model derived from [77]. Note that other analytical models, like that proposed by Papadakis et al. in [78,79], can also be used. The simple model used here can only regard the supplementary cementing materials (e.g. SF) as inert additions. Consequently, the C–S–H amounts computed in the case of SF-mixtures are expected to be underestimated (see Fig. 11). However, in the case of SF-mixtures, more relevant values can be computed by this model when using the ''equivalent'' degrees of hydration previously defined, instead of the measured degrees of hydration. This has been carried out here for CH, BH and B80-S, and the resulting values are also indicated in Fig. 11. For all the tested materials, a quite acceptable agreement is observed between the analytical and experimental methods (see Fig. 11). However, the analytical model systematically slightly overestimates the amounts, except in the case of very high W/C (CP and M25), where the C–S–H amounts are underestimated (threshold around 0.45). The values found here by both methods are lower than the values around 0.25 reported by Olson and Jennings in [76] for mature (1-year old) hcps. Only the experimental result obtained on CP

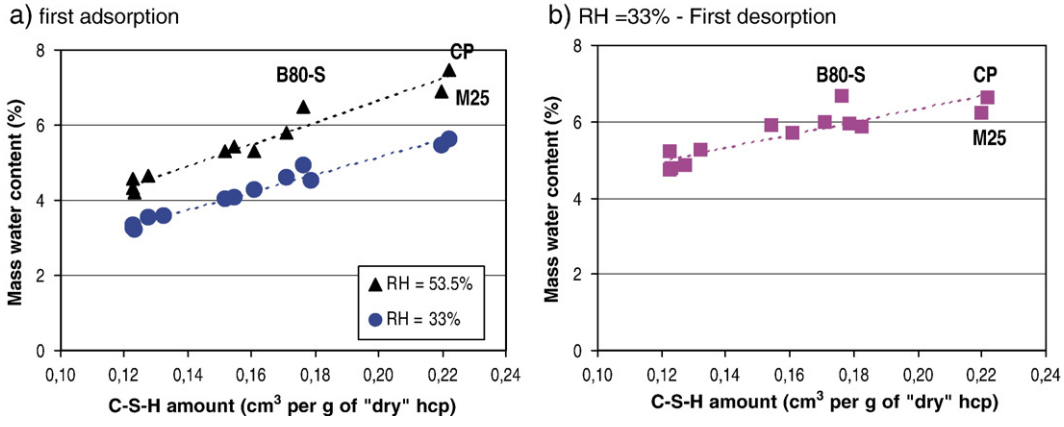

Fig. 12. Correlation between ''equilibrium'' mass water contents provided by water vapour sorption isotherms and C–S–H amount, for various hcps and concretes. The water contents are expressed in percentage per unit mass of ''dry'' hcp contained in the material.

is close to these values. This results at least from the different masses in the ''dry'' state selected for the computation of the water amounts adsorbed (''equilibrium'' mass at RH = 3% and mass after D-drying) in the case of experimental values, and probably to the lower degrees of hydration of the materials tested here.

In order to illustrate the linear relationships previously mentioned, the ''equilibrium'' mass water contents at RH=33% and at RH=53.5% provided by the WVAIs of the various tested materials are plotted *vs.* the C–S–H amounts assessed experimentally and expressed in cm^3 per g of ''dry'' hcp in Fig. 12a. Likewise, the ''equilibrium'' mass water contents at RH=33% provided by the WVDIs are plotted *vs.* the C–S–H amounts in Fig. 12b. In this last case, the water content at $T=23\pm0.1$ °C, for BO-AF, has been deduced from the experimental value at $T=44\pm0.1$ °C and from the analytical formula given in [81].

4.4.4.3. Average thickness of the multimolecular water layer adsorbed. It is possible to assess the average statistical thickness $t(h)$ of the water film adsorbed on the solid surface, from the adsorbed volume $V_{ads}(h)$ and from the BET specific surface area measured by water vapour adsorption (Eq. (1)):

$$t(h) = \frac{V_{ads}(h)}{S_{sBET}} \quad (1)$$

where h is the relative humidity.

Since the development of the ''t method'' devoted to the assessment of micropore size distribution, proposed by De Boer and Lippens [80], numerous ''t curves'' associated with nitrogen adsorption have been published in the literature, and these ones were found to be only slightly dependent on the adsorbent nature. As far as water vapour adsorption is concerned, the first ''*t* curves'' were published by Hagymassy et al. in 1969 [63]. These curves remain still now among the most relevant.

The average statistical thickness $t(h)$ of the adsorbed water film has been computed here from adsorption data according to Eq. (1) and compared to the ''*t* curve'' proposed by Hagymassy et al. in [63] for non-porous adsorbents characterized by a similar molar heat of adsorption of water molecules on their solid surface and thus by a similar BET constant than that of cementitious materials (see Fig. 13).

For RH ≤ 63.2% (r_p<3 nm), the analysis reveals a master curve: a *universal* $t(h)$ curve, which matches, whatever the material, hcp or concrete (and the moisture history, the composition of the cement, the specimen size,...), the ''t curve'' proposed by Hagymassy et al. for non-porous adsorbents. The results displayed in Fig. 13 mean that the water content rise, experimentally recorded *vs.* RH, is statistically equivalent to the increase of the thickness of a multimolecular water layer adsorbed on the solid surface, as on a non-porous adsorbent. When considering the average statistical thickness of a monomolecular water layer adsorbed (t_m=3 Å, according to [63], or t_m=2.84 Å according to some other authors), it can be deduced from Fig. 13 that below RH=22.8%, t is less than t_m. This confirms the usual assumption that strongly bound water is removed from the C–S–H (see also Ref. [33]) and explains the associated ''irreversible'' effects recorded during desorption within this very low RH range (see Section 4.2). Moreover, a linear relationship is pointed out between RH and *t*within the RH range [12% ; 63.2%]. It can hence be deduced that this is precisely the range where the ''equilibrium'' water amount adsorbed is proportional to the C–S–H amount (see the cases RH=33% and RH=53.5% in Fig. 12a). Such ''intrinsic'' features, valid for all the materials, can be very useful for the modelling of transport and degradation processes. Note that the master curve obtained at $T=23\pm0.1$ °C seems also valid for experiments performed at $T=44\pm0.1$ °C, at least for the data available here (see the results obtained for concrete BO-AF at this last temperature and displayed in Fig. 13). This seems in accordance with [20,26,81], where it is illustrated that temperature does not have much influence on the adsorption isotherm in the range of the considered temperatures.

From RH=63.2% (r_p=3 nm), a significant condensation takes place in the pore volume of normal materials, which implies the overall filling of a lot of pores. Therefore, the actual ''equilibrium'' water amount adsorbed (bulk filling) is slightly higher than the one equivalent to the increase of the thickness of a multimolecular water layer adsorbed on the solid surface (the core of the pores remains empty in this last case). As a matter of fact, the average statistical thickness $t(h)$ is above the ''*t* curve'' (see Fig. 13). The influence of mix-parameters (in particular W/C) becomes significant. Therefore, this RH value is the borderline between two domains: the (surface) multilayer adsorption range for RH ≤ 63.2%, and the (bulk) capillary absorption range for RH > 63.2% with the prominent influence of W/C within the high RH range. A linear relationship can thus be pointed out again between ''equilibrium'' adsorption water contents at RH=90.4% and W/C [33], as in the case of desorption data. Nevertheless, as illustrated in Fig. 13, the experimental $t(h)$ curves remain close to the ''*t* curve'' proposed

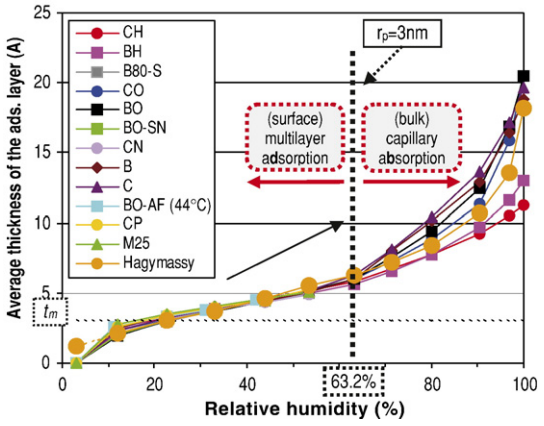

Fig. 13. Comparison between the experimental t(h) curves obtained with the various tested materials (series 1, 2, 2* and 3; 0.20 ≤ W/C ≤ 0.84; 0 ≤ SF/C ≤ 0.10) and the "*t* curve" proposed by Hagymassy in [63] for non-porous adsorbents with similar heat of adsorption (C constant of the BET equation). Some of the plots (M25, CP, BO-AF, BO-SN, CN and B80-S) have not yet reached RH=100%, since the experiments are not finished, see Fig. 9a).

in [63], which appears quite suitable to quantify the ''adsorbed'' phase thickness over the whole RH range (in particular above RH = 63.2%, where experimental data cannot be obtained), for example in view of pore size distribution assessment (see Section 4.4.2). Fig. 13 shows that a six-molecule water layer at the maximum can be adsorbed onto the internal surface of cementitious materials. As far as HP materials such as BH and CH are concerned, water adsorption is restricted by the pore sizes to about a four-molecule water layer. The hindered adsorption above RH = 63.2% is highlighted by the fact that the experimental $t(h)$ curves of CH and BH are shifted under the ''t curve'' (obtained on non-porous adsorbents). This is in agreement with the pore size distributions displayed in Fig. 6: the pore volume is extremely small for $r_p > 3$ nm.

4.4.5. Bulk porosity accessible to water

From the water content at RH = 100% deduced from the experimental WVDI ($W_{des.(RH=100\%)}$), and by assuming that this value is not very far from the value at vacuum saturated state, it is possible to deduce the (volumetric) bulk porosity accessible to water of the material Φ (in %), as follows (Eq. (2)):

$$\Phi = W_{des.(RH=100\%)} \cdot \rho_{app.dry} / \rho_l \quad (2)$$

where $\rho_{app.\ dry}$ denotes the apparent bulk mass density of the dry material and ρ_l the liquid water mass density (in kg m^{-3}).

Eq. (2), which assumes $S_l = 1$ at RH = 100%, will therefore slightly underestimate the porosity.

The values obtained for the various materials tested are compared in Fig. 14 to:

- the "theoretical" porosities computed from the W/C, the degree of hydration of the cement at the appropriate age (measured or estimated), the mineralogical composition of the cement, and the water amount required for full hydration of each mineralogical compound (see Ref. [33,82]),
- the porosities measured by means of hydrostatic weighing (vacuum saturation, weighing in water and in the air, and drying [60]),
- the porosities measured by means of gamma-ray attenuation (see Section 5.2.3), when these data are available.

$\rho_{app.dry}$ has been measured by hydrostatic weighing (or by both hydrostatic weighing and gamma-ray attenuation measurement when available) for each material. A very good agreement is observed. However, as expected and as the hydrostatic weighing technique involves vacuum saturation of the samples, the porosities measured by this technique are slightly higher than the values deduced from Eq. (2), for most of the materials. The more significantly higher values measured by hydrostatic weighing in the case of PCB and B30-A can be explained by the presence of a significant quantity of big voids (unable to be quantified by sorption). This has been confirmed in the case of PCB by microscope observations [35], and probably results from the casting procedure. Conversely, the difference is very small in the case of HP materials, as a result of the very small difference between vacuum saturated state and ''equilibrium'' state at RH = 100% for these materials (as illustrated for example in Section 5 by gamma-ray attenuation measurements on B80-S, see Fig. 19). The lower value obtained in the case of CP can be explained by the difficulty to prepare homogeneous "big" samples with such porous hcps. The ''theoretical'' computation, also based on the assumption $S_l = 1$ at RH = 100%, provides very similar values as does Eq. (2), except in the case of CP, M25, B80-S and BH. The higher ''theoretical'' values obtained in the case of CP and M25 (materials with very high W/C), compared to those measured by desorption, hydrostatic weighing or gamma ray, are certainly the result of bleeding, which yields a lower actual W/C in the specimens than the theoretical one. The lower "theoretical" values obtained in the case of B80-S and BH, compared to those measured by desorption, hydrostatic weighing or gamma ray, are maybe the result of the difficulty to assess an accurate value of degree of hydration with this type of concretes.

4.4.6. C–S–H ''gel'' porosity and capillary porosity

With the assumption (based upon the BJH pore size distributions displayed in Section 4.4.2, see Fig. 6) that the C–S–H ''gel'' pore volume can be roughly associated with $r_p \leq 5$ nm (*i.e.* RH ≤ 76%), it is possible to deduce the C–S–H ''gel'' porosity in the materials tested here, from the water

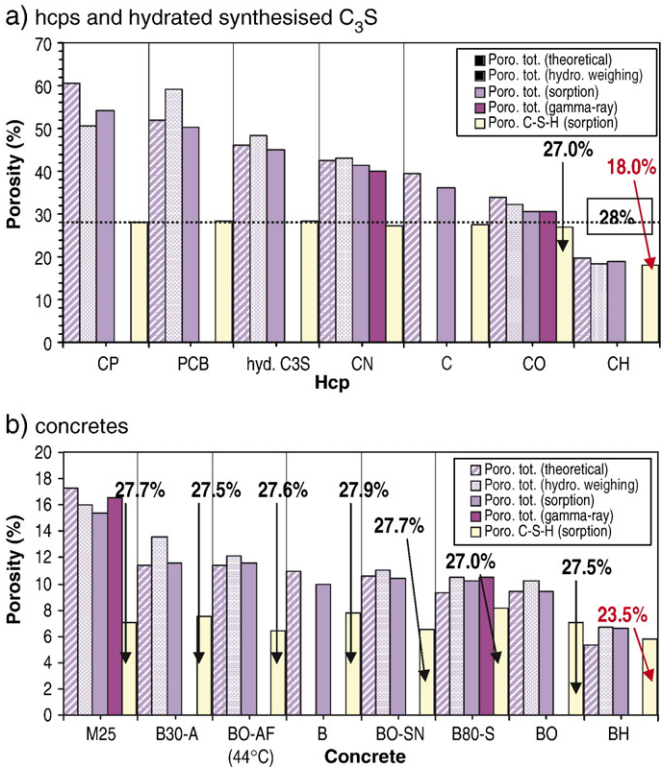

Fig. 14. Bulk porosity accessible to water and porosity of the C–S–H ''gel'', deduced from the experimental water vapour desorption isotherms for the various tested materials. Comparison with the porosity measured by hydrostatic weighing, the porosity measured by gamma-ray attenuation and the ''theoretical'' porosity deduced from the mix-composition and the degree of hydration. C–S–H "gel" porosity values, expressed in percentage per unit volume of hcp, are also reported in the figure.

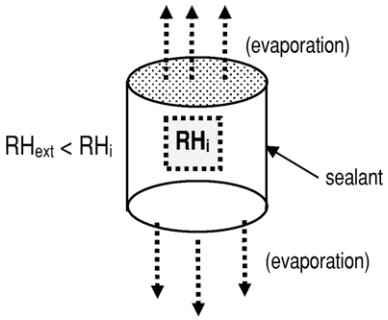

Fig. 15. D isothermal drying test at RH_{ext}=53.5% or 71.5% and at T=21±1 °C on mature samples in laboratory.

content at RH=76% provided by the experimental first desorption isotherm. The results are reported in Fig. 14, highlighting the C–S–H ''gel'' porosity proportion (and therefore the capillary porosity proportion) in the various materials. A significant contribution to the total porosity is recorded (from 45 to 95%), in particular in the case of HP materials, which consequently display a very low capillary porosity, as previously mentioned in this paper.

The values found here for most of the hcps and concretes, ranging from 27.0 to 28.4%, are in agreement with the model proposed by *Powers and Brownyard* [23], which states that, whatever the W/C and the degree of hydration of the cement, the C–S–H ''gel'' porosity of hcps has the intrinsic value of 28%. In addition, according to the results presented here, the statement can be extended to concretes. Within this range, the lowest value (27.0%) is found for concrete B80-S and hcp CO (W/C=0.35).

Nevertheless, exceptions are experimentally pointed out here: particularly low values are found for concrete BH (23.5%) and hcp CH (18.0%), materials with very low W/C and which incorporate SF. These results are in agreement with the BJH pore size distributions of these materials (the pore radii are lower than 2 nm, see Section 4.4.2) and microscope observations, which reveal that in these materials the C–S–H ''gel'' is mainly constituted of dense (HD) products (see Section 4.4.3). In addition, the values found here for these materials seem consistent with the model proposed by Jennings et al., which states that the porosity of HD C–S–H is 24% and the nanoporosity (porosity internal to C–S–H globules) is 18%, as reported in [53,57,83]. It is worth mentioning that such lower C–S–H ''gel'' porosity values than the one accepted since Powers and Brownyard [23] have to be taken into account in macroscopic models.

The capillary porosity values deduced from WVDIs (as bulk porosity minus C–S–H ''gel'' porosity) can be compared to the theoretical values calculated from empirical formulas proposed in the literature. For example, by using the degrees of hydration reported in Table 2 and the formulas proposed in [85] based on the work of *Powers and Brownyard* [23], the values 26.0%, 15.0% and 4.2% are found for the normal hcps CP, CN and CO (25.9%, 14.2% and 3.5% are deduced from the WVDIs, respectively). For CP and CN, the average of the water-filled and total porosity capillary values is reported, whereas for CO only the water-filled capillary porosity value has been taken into account. Likewise, for the hydrated synthesised C_3S, 16.8% has been directly calculated from its theoretical composition (and by considering the C–S–H as $C_{1.7}SH_4$), against 16.7% deduced from the WVDI. Therefore, a good agreement is pointed out between calculated and experimental values.

5. Analysis of moisture profiles under laboratory and in-situ drying conditions

5.1. Background and contents of the study

External drying takes place in concrete when the material is submitted to a lower environmental RH than its internal one. This process affects the surface zone of many engineering structures. In order to confirm the findings deduced from the WVSIs and to investigate their consequences on actual long-term external drying behaviour of concrete, moisture profiles have been measured by gamma-ray attenuation in cores drilled out from various concrete structures exposed to natural weathering conditions. Likewise, the evolution of the moisture profile as a function of time has been monitored in mature samples of normal and HP materials submitted to 1-D isothermal drying experiments in well-defined laboratory conditions (see Fig. 15).

5.2. Experiments

5.2.1. Investigations carried out under in-situ conditions

∅75×150-mm cores have been drilled out from RC test specimens (concretes M25 and M75-FS) exposed for 4 years to two types of natural environments [37,38]:

- a urban environment (Melun, France): the average temperature (within a year) is about 11.6 °C and the average RH is 77–80% (it ranges from 40 to 95%). The structural elements are not sheltered from rain. Core sampling was performed in early summer on the side oriented southwest,
- a road and cold environment (Maurienne, French Alps): the structural elements are installed along the road. They are exposed to freezing and thawing cycles and to the spraying of deicing salts. On this site, the minimum (resp. maximum) temperature (within a year) is about 3 °C (resp. 33 °C) and the average temperature (within a year) ranges from 7.5 to 8.8 °C. The concrete elements are covered by snow about 30 days a year.

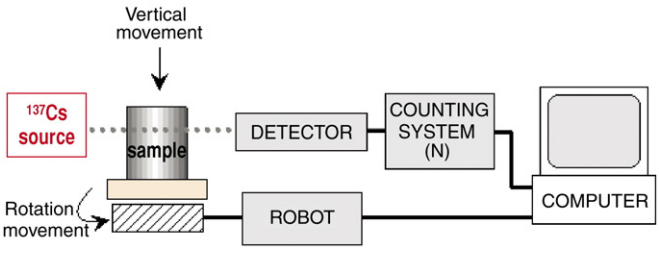

Fig. 16. Simplified scheme of the gamma-ray attenuation measurement system.

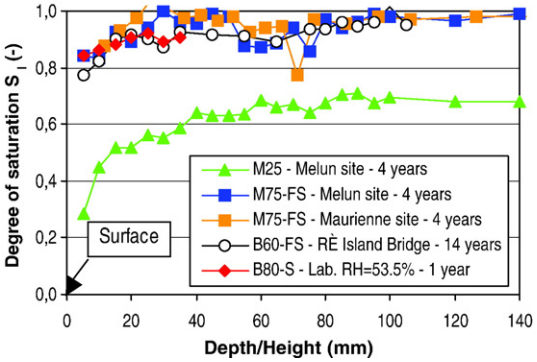

Fig. 17. Gamma-ray moisture (expressed as degree of liquid water saturation S_l) profiles of various concretes, measured in cores drilled out from structures in various natural environments. Comparison with results obtained on concrete B80-S, after 1-year exposure to RH = 53.5% in laboratory (after water curing and vacuum saturation).

In addition, ∅75 × 115-mm cores have been drilled out from the deck of the Ré Island Bridge (concrete B60-FS) at the age of 14 years [39]. The average temperature (within a year) is about 13.5 °C on this site and the average RH (within a year) ranges from 76 to 79%.

5.2.2. 1-D isothermal drying experiments carried out under laboratory conditions

After casting in laboratory and wet sawing, samples of concretes M25 (∅110 × 100 mm) and B80-S (∅110 × 70 mm), and of hcps CO and CN (∅70 × 100 mm) have been submitted to 1-D isothermal external drying at RH = 53.5% (and also at RH = 71.5% in the case of M25) and at $T = 21 \pm 1$ °C. Some samples of hcp CO were prepared with 1.5 or 3% NaCl per unit mass of cement. In order to avoid any influence of self-desiccation during the external drying process, the samples were water cured for several months before exposure to drying. In addition, in order to insure 1-D drying, the cylindrical samples were sealed by two superposed self-adhesive aluminium foil sheets, except the two opposite plane sides, before submitting them to drying (see Fig. 15).

5.2.3. Gamma-ray attenuation measurements

Gamma-ray attenuation measurements are based on the attenuation by a material of the gamma-photons emitted by a radioactive source. The bulk mass density ρ of the material (in kg m^{-3}) can be calculated from the parameters directly assessed from gamma-ray measurements: the number N_0 of emitted photons in free air (in impulses/s) and the number N of photons recorded after crossing a thickness x (in m) of the material (see Fig. 16), according to Beer–Lambert law (see Eq. (3)) [33,38]:

$$\rho = \frac{1}{\mu \cdot x} \cdot \ln\left(\frac{N_0}{N}\right) \tag{3}$$

where μ is the mass absorption coefficient of the material at the actual moisture state (in m^2 kg^{-1}) associated with the energy of the radioactive source used (here Cesium 137).

5.3. Experimental results under in-situ conditions — comparison with laboratory results

The moisture (degree of liquid water saturation) profiles, obtained by gamma-ray attenuation measurements on cores drilled out from the RC test specimens (concretes M25 and M75-FS) after 4-year exposure on Melun and Maurienne sites and from the Ré Island Bridge (concrete B60-FS) after 14 years, are presented in Fig. 17. They are compared in this figure to the profile obtained on the laboratory sample B80-S, after 1-year exposure to RH = 53.5% in laboratory (after water curing and vacuum saturation) (see Section 5.4).

The natural drying (more exactly the daily and seasonal drying-wetting cycles) of concrete, which starts from the surface zone exposed to the environmental conditions, as well as the resulting microstructural characteristics and their gradient *vs.* the depth, explain the reduction in the degree of saturation recorded within the surface zone whose thickness depends on the mixture. The experimental results highlight very different profiles for HPCs compared to the low-grade concrete M25, even under the same environmental conditions (see Fig. 17). HPCs, such as for

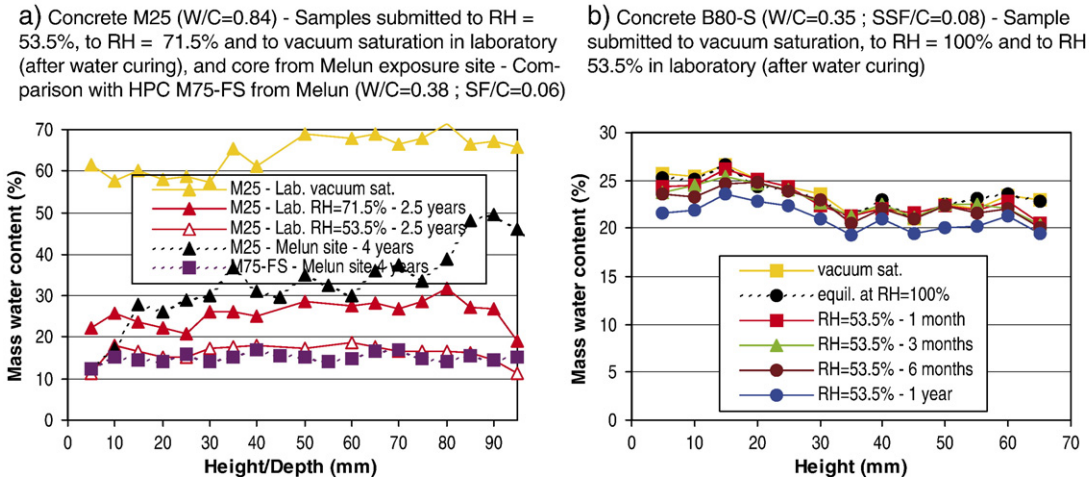

Fig. 18. Gamma-ray moisture (expressed as mass water content) profiles under laboratory conditions at $T = 21 \pm 1$ °C and comparison with results obtained in natural environments. The water contents are expressed in percentage per unit mass of "dry" hcp contained in the materials.

example concretes M75-FS (porosity accessible to water measured on cores equal to 8.4%), B60-FS (porosity 10.8%) or B80-S, are weakly sensitive to the environmental conditions. As a matter of fact, at a given depth, the degrees of liquid water saturation of the various concretes measured in various natural environments (and in laboratory) and at various ages are very similar (see Fig. 17). These concretes keep in the course of time a very high degree of saturation, within the surface and the inner zones (0.80–0.85 within the surface zone and 0.95–1 within the inner zone) (see Fig. 17). These findings can be mainly attributed to the peculiar shape of the WVSIs, which are rather flat within a broad RH range from RH=100%, as previously detailed (see Figs. 1b, 3 and 4), in Section 4.3).

According to the gamma-ray results (see Fig. 18a), after 4-year exposure in the Melun site, the water content in the low-grade concrete M25 test specimen is about 40% (by unit mass of ''dry'' hcp) in its inner zone, and 12% at 5 mm from the surface. Note that his last value matches the value obtained in laboratory at the surface of the sample exposed to RH=53.5% (see Fig. 18a and Section 5.4). For the HPC M75-FS in the same conditions, the respective values are 15.5% and 12% (see Fig. 18a). The associated internal RHs of M25 and M75-FS can be calculated from these in-situ gamma-ray water contents and from the WVDIs provided in Fig. 3b by assuming that M75-FS has a similar WVDI as B80-S. The deduced internal RHs are 92% (inner zone) and 54% (surface zone) for M25, and 75% and 55%, respectively, for M75-FS. It can be deduced from these results that:

- the internal RH calculated from gamma-ray measurement and WVDI within the surface zone of drilled cores of concretes M25 and M75-FS is consistent with the environmental conditions (by assuming that the microstructural changes induced by any early-age drying are negligible), as the external RH was around 55% at the time of drilling,
- self-desiccation yielded RH≈75–80% within the inner zone of the HPC, since this zone does not seem affected by external drying. This experimental value is in agreement with the literature [7,8,30]. In addition, measurements in laboratory at $T=21\pm1$ °C by RH-probes provided an average internal RH value of 82% on the same type of concretes in sealed conditions. This highlights that strong self-desiccation is compatible with a high degree of liquid water saturation (as a result of the very fine pore network of HPCs). Note moreover that the same RH-probe measurements in laboratory provided an average internal RH value of 95% for M25. This value seems consistent with the one measured in situ in the inner zone of the test specimen M25 (92%).

All of these results illustrate the excellent agreement between laboratory (water vapour and drying tests) and in-situ data.

5.4. Experimental results under laboratory (drying) conditions

Significant discrepancies between normal and HP materials are also found in the case of 1-D drying under same laboratory conditions, after sealed or water curing. For example (see Fig. 18b), after 1-year drying at RH=53.5% (after 1-year water curing and vacuum saturation), even at 5 mm from the surface zone, the gamma-ray water contents in HPC B80-S are far from ''equilibrium'' state (the lowest value measured is 19%, see Fig. 18b, against 11% provided by the WVDI of the material at RH=53.5%, see Fig. 3b). A flat profile along with a high degree of saturation are observed, very similar to those obtained at short drying times (see Fig. 19a). Nearly no evolution is recorded from a few-day to 6-month drying. Similar results were found in [15] for CH and BH after sealed curing. Moreover, similar degrees of saturation are measured as under natural conditions (see Fig. 17). Furthermore, the gamma-ray data point out only a slight difference between vacuum-saturated state and "equilibrium" state at RH=100% in the case of this material. Conversely, for more porous concretes, a significant shift of the profile is observed as a function of the drying time. After 2.5-year exposure, the gamma-ray water contents obtained within the surface zone of M25 samples submitted to 1-D drying at RH=71.5% (22% by unit mass of ''dry'' hcp) or RH=53.5% (11.25%) in laboratory (after 1-year water curing) (see Fig. 18a) match the ''equilibrium'' values provided by the WVDI of the material (21% and 11.5%, at the respective RHs, see Fig. 3b). Note that a negligible difference is recorded between the profiles at 2 and 2.5 years (see Fig. 19b), confirming thereby a state close to equilibrium. See also the

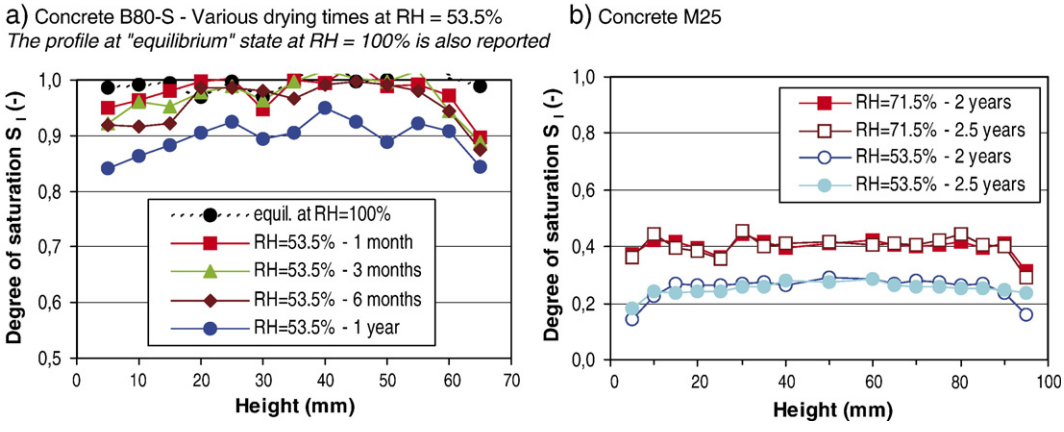

Fig. 19. Gamma-ray moisture (expressed as degree of liquid water saturation S_l) profiles of samples submitted to RH=53.5% (M25 and B80-S) and to RH=71.5% (M25) in laboratory at $T=21\pm1$ °C (after water curing).

results for CO and BO after sealed curing in [15]. In addition, the results exhibit a low degree of saturation (see Fig. 19b), as a result of the high porosity of this material. Very large differences are observed between the water content profiles measured at vacuum-saturated state and after 2.5-year exposure at RH = 53.5% (or at RH = 71.5%) (see Fig. 18a). Moreover, a flat profile is observed, but only in the long term and as a result of an efficient drying, which yields a state close to equilibrium within the whole sample (17% by unit mass of ''dry'' hcp is recorded after 2.5-year exposure at RH = 53.5% within the inner zone, see Fig. 18a). Same conclusions can be drawn in laboratory as those previously deduced from the study carried out under natural conditions (where external and internal drying are concomitant). HPCs are weakly affected by environmental variations within a broad RH range, as a main result of the peculiar shape of their WVSIs, which induces in particular a very small moisture content gradient (driving force) between surface and inner zones at the starting time of the drying process/experiment. When the sample has been stored in sealed conditions prior to the drying test, the strong self-desiccation may emphasize this phenomenon [14].

Fig. 20 displays the moisture profiles obtained on laboratory samples of hcps CO (mixed with or without NaCl) and CN, submitted to 1-D isothermal external drying at RH = 53.5% after water curing. After 6-year drying, the hygral state is not far from "equilibrium" at RH = 53.5% for CO and CN, and the gamma-ray results confirm the "equilibrium" water content values derived from the WVDIs at this RH (≈ 9%, see Fig. 8a). In addition, the gamma-ray results confirm the fact that the "equilibrium" values are nearly the same at this RH for the hcps CO and CN (RH range where the WVDIs are similar, see Fig. 8a), even if the profiles at higher moisture states were significantly different (RH range where the isotherms are very dependent of W/C, see Fig. 8). For example, 27% is found by gamma-ray at saturated state and 26% is measured by sorption at RH = 100% for CN, against 19% and 18%, respectively for CO.

Moreover, Fig. 20 illustrates that the influence of the initial presence of NaCl is not negligible: higher water contents (and degrees of saturation) are observed for CO mixed with 3% NaCl than for CO. More precisely, within the high RH range the W/C

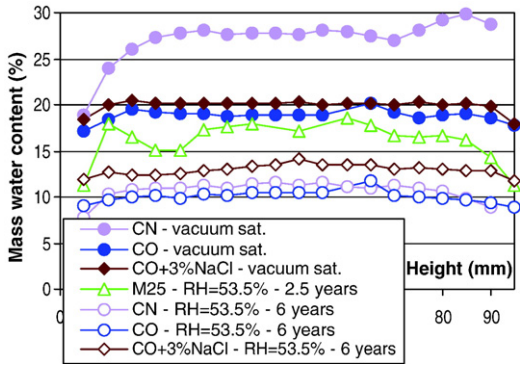

Fig. 20. Gamma-ray moisture (expressed as mass water content) profiles of samples of hcps CO (W/C = 0.35, with and without 3% NaCl per unit mass of cement) and CN (W/C = 0.45) submitted to RH = 53.5% in laboratory at $T = 21 \pm 1$ °C (after water curing), and comparison with concrete M25. The water contents are expressed in percentage per unit mass of "dry" hcp contained in the materials.

effect appears clearly prominent, but not within the mid RH range. Consequently, the ''coupling'' moisture-NaCl (or water-ions) has to be taken into account in the modelling of moisture transport, even for materials with low W/C (and thus weakly permeable), when salts (from seawater or deicing salts) are initially present.

Furthermore, these laboratory results highlight again the perfect consistence between the (equilibrium) desorption and gamma-ray (profile) data obtained respectively on 1- to 3-mm and 70- to 100-mm thick specimens.

6. Concluding remarks

Various results are presented in this paper as regards the analysis of the drying-wetting process and its relation to pore structure. In particular, the influence of W/C has been investigated on moisture properties (and microstructural characteristics) for a broad range of normal and HP hardened cement pastes and concretes. A database, which includes results from both laboratory and in-situ exposure, is available. Its practical interest is obvious, in particular to improve durability of RC structures (e.g. optimization of concrete mixtures, curing procedures and structural design). Likewise, the results are useful for further researches upon the analysis and the modelling of transport/degradation processes and associated deformations, on a physical basis.

Water vapour desorption-adsorption isotherms (WVSIs) can be regarded as the "hygro-structural" identity card of the material. Therefore, they appear as essential tools for durability evaluation and prediction and can thus be included in a *toolkit* for durability evaluation, within the framework of a performance-based durability approach [84]. These data not only provide equilibrium moisture properties but also allow a pore structure analysis in the mesopore range and the assessment of the C–S–H ''gel'' porosity and amount (description of the nanostructure). Such parameters are hardly accessible by most of the other usual techniques. This highlights the specific interest of WVSIs for high-tech concretes such as HPCs or ultra-high-performance fiber-reinforced concretes. In addition to the parameters quantified in this paper, other characteristics, such as the energy state of the pore water and the fractal dimension of the C–S–H ''gel'', can be assessed [33]. In this paper, it has been found that the presence of aggregates does not influence WVSIs. Moreover, the analysis of the desorption–adsorption hysteresis has shown that no ''permanent'' irreversible process occurred during the water vapour sorption processes. Furthermore, the WVSIs can be partitioned in different ranges, which are influenced or not by W/C. A unique partition of WDSIs has been pointed out, valid for every material tested, from hydrated synthesised C_3S to HPC extracted from real bridge. Likewise, a master curve has been exhibited as regards the average adsorbed water layer thickness *vs.* RH, for RH ≤ 63.2%. In addition, the peculiarities of HP materials as regards hygral behaviour and microstructure have been highlighted:

- within the high RH range, significant lower water contents are measured than for normal materials, and large RH changes induce only slight variations of water content, as a result of the very small pore volume involved in the wetting-drying process,

- these materials exhibit a significantly higher degree of liquid water saturation within the whole RH range, compared to normal materials,
- the C–S–H ''gel'' seems mainly constituted of dense (HD or inner-like) products.

The database and the ''intrinsic'' properties pointed out here (e.g. master curves) can easily be used to predict the behaviour of any (not tested) normal or HP concrete mixture designed for a structure. For example, average WVSIs along with standard deviation could be computed by means of analytical or numerical methods and could then be included as input data in transport/degradation predictive models, without performing any additional sorption experiment, which would be very time consuming and therefore not appropriate to the field timescale. Likewise, "critical" isotherms as regards given actual environments/degradations of structures could be defined upon a probabilistic approach [17].

The in-situ internal RH has been assessed from WVDI and gamma-ray moisture profile on drilled cores, exhibiting that a high degree of saturation is compatible with a strong self-desiccation for HPCs, as a result of their very fine pore structure. In addition, the very similar moisture profiles and the high degrees of liquid water saturation recorded by gamma-ray in these materials, whatever the mixture, the age and the environmental (laboratory or in-situ) conditions, confirm that HPCs are weakly affected by weathering conditions, except maybe within a very thin zone at the vicinity of the exposed surface (depth <5 mm). This will be an advantage as regards durability, under the condition of an appropriate (external or internal) curing procedure.

At last, a perfect consistence has been pointed out in this paper between the water contents provided, on the one hand, by desorption experiments on 1- to 3-mm thick specimens (granules or slices), and on the other hand, by gamma-ray attenuation measurements on 70- to 150-mm thick cylinders tested in laboratory or in natural weathering conditions.

Acknowledgments

The author gratefully acknowledges J. Gawsewitch and J.F. Bouteloup, who contributed to the long-term experimental work, as well as P. Roussel who carried out gamma-ray attenuation measurements. The author thanks also Dr. T. Chaussadent for his collaboration in the microstructural characterization.

References

[1] H. Wiering, Longtime studies on the carbonation of concrete under normal outdoor exposure, Proc. of RILEM Seminar, Hannover, Germany, 1984, pp. 239–249.
[2] K. van Balen, D. van Gemert, Modelling lime mortar carbonation, Mat. Struct. 27 (1994) 393–398.
[3] M. Thiery, V. Baroghel-Bouny, G. Villain, P. Dangla, Numerical modeling of concrete carbonation based on durability indicators, in: V.M. Malhotra (Ed.), Proceedings of the 7th CANMET/ACI International Conference on Durability of Concrete, may 28 – june 3, 2006, Montreal (Québec), Canada, ACI, 2006, pp. 765–780, SP-234.
[4] S.K. Roy, K.B. Poh, D.O. Northwood, Durability of concrete. Accelerated carbonation and weathering studies, Build. Environ. 34 (1999) 597–606.
[5] F.J. Ulm, O. Coussy, L. Kefei, C. Larive, Thermo-chemo-mechanics of ASR expansion in concrete structures, J. Eng. Mech. 126 (3) (2000) 233–242.
[6] O.M. Jensen, F. Hansen, Autogenous relative humidity change in silica-fume-modified cement paste, Adv. Cem. Res 7 (25) (1995) 33–38.
[7] V. Baroghel-Bouny, Experimental investigation of self-desiccation in high-performance materials - Comparison with drying behaviour, in: B. Persson, G. Fagerlund (Eds.), Proc. of 1st Int. Research Seminar 'Self-Desiccation and its Importance in Concrete Technology', june 10th, 1997, Lund, Sweden, 1997, pp. 72–87.
[8] B. Persson, Consequences of cement constituents, mix composition and curing conditions for self-desiccation in concrete, Mat. Struct. 33 (2000) 352–362.
[9] F.J. Ulm, F. Le Maou, C. Boulay, Creep and shrinkage coupling: new review of some evidence, Rev. Fr. Genie. Civ. 3 (3/4) (1999) 21–37.
[10] E.J. Sellevold, Ø. Bjøntegaard, H. Justnes, P.A. Dahl, High-performance concrete: early volume change and cracking tendency, Proc. of Int. RILEM Symp. on Thermal Cracking at Early Ages, Munich, Germany, E. & F.N. Spon, London, 1994, pp. 229–236.
[11] B. Pease, A.B. Hossain, J. Weiss, Quantifying volume change, stress development and cracking due to early-age autogenous shrinkage, in: O.M. Jensen, D.P. Bentz, P. Lura (Eds.), Proc. of ACI Fall 2002 Convention, Session ''Autogenous Deformation of Concrete'', oct. 27 – nov. 1, 2002, Phoenix, Arizona, USA, ACI, march 2004, pp. 23–38, SP-220.
[12] L. Stefan, F. Benboudjema, F. Robert, M. Moranville, Drying and shrinkage — Influence of induced cracking (in French), Proc. of Colloque National sur les Propriétés de Transfert dans les Géomatériaux ''Transfert 2006'', feb. 1–2, Villeneuve d'Ascq, France, 2006.
[13] V. Baroghel-Bouny, Water vapour sorption experiments on hardened cementitious materials. Part II: Essential tool for assessment of transport properties and for durability prediction, Cem. Concr. Res. 37 (2007) 438–454.
[14] V. Baroghel-Bouny, M. Mainguy, O. Coussy, Isothermal drying process in weakly permeable cementitious materials — Assessment of water permeability, in 'Materials science of concrete', Special volume: 'Ion and mass transport in cement-based materials' (Ed. by R.D. Hooton, M.D.A. Thomas, J. Marchand and J.J. Beaudoin, Series Ed. J.P. Skalny, American Ceramic Society, 2001), pp 59–80.
[15] V. Baroghel-Bouny, M. Mainguy, T. Lassabatere, O. Coussy, Characterization and identification of equilibrium and transfer moisture properties for ordinary and high-performance cementitious materials, Cem. Concr. Res. 29 (1999) 1225–1238.
[16] B. Bary, A. Sellier, Coupled moisture-carbon dioxide-calcium transfer model for carbonation of concrete, Cem. Concr. Res. 34 (10) (2004) 1859–1872.
[17] F. Duprat, A. Sellier, X.S. Nguyen, Consequences of moisture state uncertainty of concrete on carbonation: probabilistic approach (in French), Proc. of Colloque National sur les Propriétés de Transfert dans les Géomatériaux ''Transfert 2006'', feb. 1–2, Villeneuve d'Ascq, France, 2006.
[18] S. Brunauer, P.H. Emmett, E.J. Teller, Adsorption of gases in multimolecular layers, J. Am. Chem. Soc. 60 (1938) 309–319.
[19] G.L. Aranovitch, New polymolecular adsorption isotherm, J. Colloid Interface Sci. 141 (1) (1991) 30–43.
[20] Y. Xi, Z.P. Bazant, H.M. Jennings, Moisture diffusion in cementitious materials, Adsorption Isotherms, vol. 1, ACBM, 1994, pp. 248–257.
[21] J. Adolphs, M.J. Setzer, Description of gas adsorption isotherms on porous and dispersed systems with the excess surface work model, J. Colloid Interface Sci. 207 (1998) 349–354.
[22] B. Coasne, K.E. Gubbins, R.J.-M. Pellenq, A Grand Canonical Monte Carlo study of adsorption and capillary phenomena in nanopores of various morphologies and topologies: testing the BET and BJH characterization methods, Part. Part. Syst. Charact. 21 (2004) 149–160.
[23] T.C. Powers, T.L. Brownyard, Studies of the physical properties of hardened Portland cement paste, Portland Cem. Assoc. 22 (1948) 276–287.
[24] R.F. Feldman, Sorption and length-change scanning isotherms of methanol and water on hydrated Portland cement, Proc. of 5th Int. Congress on the Chemistry of Cement, vol. 3, Cem. Assoc. of Japan, Tokyo, 1968, pp. 53–66.

[25] R. Badmann, N. Stockhausen, M.J. Setzer, The statistical thickness and the chemical potential of adsorbed water films, J. Colloid Interface Sci. 82 (2) (1981) 534–542.
[26] F. Radjy, E.J. Sellevold, K.K. Hansen, Isosteric vapor pressure — Temperature data for water sorption in hardened cement paste: enthalpy, entropy and sorption isotherms at different temperatures, Report BYG·DTU R-057, Technical Univ. of Denmark, 2003, 52 pp.
[27] S. Tada, K. Watanabe, Dynamic determination of sorption isotherm of cement based materials, Cem. Concr. Res. 35 (2005) 2271–2277.
[28] Xu Aimin, Water desorption isotherms of cement mortar with fly ash, Nord. Concr. Res. 8 (1989) 9–23.
[29] E. Atlassi, Some moisture sorption properties of silica fume mortar, Proc. of Int. 4th CANMET/ACI Conf. on Fly Ash, Silica Fume, Slag and Natural Pozzolans in Concrete, Istanbul, Turkey, vol. 2, may 1992, pp. 903–919.
[30] K. Norling-Mjörnell, A model of self-desiccation in high performance concrete, in: B. Persson, G. Fagerlund (Eds.), Proc. of 1st Int. Research Seminar 'Self-Desiccation and its Importance in Concrete Technology', june 10th, 1997, Lund, Sweden, 1997, pp. 141–157.
[31] J. Adolphs, A. Schreiber, Microstructural characterisation of Ultra-High Performance Concrete, in: Schmidt, Fehling, Geisenhanslüke (Eds.), Proc. of Int. Symp. on Ultra High Performance Concrete, sept. 13–15, 2004, Kassel, Germany, Structural Materials and Engineering, Series, vol. 3, 2004, pp. 265–271.
[32] V. Baroghel-Bouny, T. Chaussadent, Pore structure characterization of hardened concrete from water vapour sorption isotherms (in French), Bull. Lab. Ponts Chaussees 187 (1993) 69–75.
[33] V. Baroghel-Bouny, Characterization of cement pastes and concretes — Methods, analysis, interpretations (in French), Ph.D. Dissertation (LCPC Publ., Paris, 1994), 468 p.
[34] T. Chaussadent, V. Baroghel-Bouny, H. Hornain, N. Rafaï, A. Ammouche, Effect of water-cement ratio of cement pastes on microstructural characteristics related to carbonation process, in: V.M. Malhotra (Ed.), Proc. of 5th Int. CANMET/ACI Conf. on Durability of Concrete, June 4–9, 2000, Barcelona, Spain, vol. I, ACI, 2000, pp. 523–537, SP 192.
[35] V. Baroghel-Bouny, A. Ammouche, H. Hornain, Cementitious binders: analysis of the microstructure and transport properties (in French), in: V. Baroghel-Bouny (Ed.), Transferts dans les bétons et durabilité, Special Issue of Revue Française de Génie Civil, vol. 5 (2–3), Hermès Science Publications, Paris, 2001, pp. 149–177.
[36] V. Baroghel-Bouny, P. Mounanga, A. Khelidj, A. Loukili, N. Rafai, Autogenous deformations of cement pastes. Part II: W/C effects, micro–macro correlations, and threshold values, Cem. Concr. Res. 36 (1) (2006) 123–136.
[37] V. Baroghel-Bouny, F. de Larrard, In place durability assessment for the next millenium — Long-term study, in: V.M. Malhotra (Ed.), Proc. of 5th Int. CANMET/ACI Conf. on Durability of Concrete, june 4–9, 2000, Barcelona, Spain, vol. I, ACI, 2000, pp. 319–338, SP 192.
[38] V. Baroghel-Bouny, J. Gawsewitch, P. Belin, K. Ounoughi, S. Arnaud, G. Olivier, B. Bissonnette, Ageing of concretes in natural environments: an experiment for the 21st century. iv — Results on cores extracted from field-exposed test specimens of various sites at the first times of measurement, Bull. Lab. Ponts Chaussees 249 (2004) 49–100.
[39] V. Baroghel-Bouny, Specificities of high-performance concretes — Microstructural characteristics and durability-related properties, evaluated in laboratory and in natural conditions (in French), Etudes et Recherches des LPC, Série Ouvrages d′art, vol. OA 44, LCPC, Paris, sept. 2004, 76 pp.
[40] K.S.W. Sing, D.H. Everett, R.A.W. Haul, L. Moscou, R.A. Pierotti, J. Rouquerol, T. Siemieniewska, IUPAC (Recommendations 1984), Reporting physisorption data for gas/solid systems with special reference to the determination of surface area and porosity, Pure Appl. Chem. 57 (4) (1985) 603–619.
[41] D.L. Kantro, S. Brunauer, C.H. Weise, Adv. Chem. Ser. 33 (199) (1961).
[42] S.E. Pihlajavaara, Estimation of drying of concrete at different relative humidities and temperatures of ambient air with special discussion about fundamental features of drying and shrinkage, in: Z.P. Bazant, F.H. Wittmann (Eds.), Creep and Shrinkage in Concrete Structures, John Wright & Sons Ltd, 1982, pp. 87–108.
[43] G. Villain, V. Baroghel-Bouny, J.F. Bouteloup, Assessment of water vapour diffusion coefficient in carbonated and non-carbonated concretes (in French), Proc. of Journées ''Durabilité 2006'', may 15–16, Paris, France, 2006.
[44] B.F. Johannesson, Prestudy on diffusion and transient condensation of water vapor in cement mortar, Cem. Concr. Res. 32 (2002) 955–962.
[45] B. Perrin, V. Baroghel-Bouny, L. Chemloul, Methods of determination of the hydric diffusivity of hardened cement pastes (in French), Mat. Struct. 31 (208) (1998) 235–241.
[46] O.C.G. Adan, Determination of moisture diffusivities in gypsum renders, Heron 40 (3) (1995) 201–215.
[47] K.K. Hansen, V. Baroghel-Bouny, D. Quenard, H. Künzel, Water vapor absorption isotherms for porous building materials, Proc. of Int. Symp. on Moisture Problems in Building Walls, sept. 11–13, Porto, Portugal, 1995, pp. 248–257.
[48] M.C. Garci Juenger, H.M. Jennings, The use of nitrogen adsorption to assess the microstructure of cement paste, Cem. Concr. Res. 31 (2001) 883–892.
[49] A. Korpa, R. Trettin, The influence of different drying methods on cement paste microstructures as reflected by gas adsorption: comparison between freeze-drying (F-drying), D-drying, P-drying and oven-drying methods, Cem. Concr. Res. 36 (2006) 634–649.
[50] L. Konecny, S.J. Naqvi, The effect of different drying techniques on the pore size distribution of blended cement mortars, Cem. Concr. Res. 23 (5) (1993) 1223–1228.
[51] V. Baroghel-Bouny, T. Chaussadent, Transfers within concrete and structural durability: overview of five years of research and outlook for the future, Bull. Lab. Ponts Chaussees 250–251 (2004) 115–133.
[52] J.J. Thomas, H.M. Jennings, A.J. Allen, The surface are of hardened cement pastes as measured by various techniques, Concr. Sci. Eng. 1 (1999) 45–64.
[53] H.M. Jennings, A model for the microstructure of calcium silicate hydrate in cement paste, Cem. Concr. Res. 30 (1) (2000) 101–116.
[54] V. Baroghel-Bouny, B. Perrin, L. Chemloul, Experimental determination of moisture properties of hardened cement pastes, showing hysteresis effects (in French), Mat. Struct. 30 (200) (1997) 340–348.
[55] L.J. Parrot, An examination of two methods for studying diffusion kinetics in hydrated cements, Mater. Constr. 17 (98) (1982) 131–137.
[56] E. Helsing-Atlassi, Influence of silica fume on the pore structure of mortar when measured by water vapour sorption isotherms, in: H.M. Jennings, J. Kropp, K. Scrivener (Eds.), Proc. of NATO/RILEM Workshop on the Modelling of Microstructure and its Potential for Studying Transport Properties and Durability, July 10–13, 1994, Saint-Rémy-lès-Chevreuse, France, NATO ASI Series E: Applied Sciences, vol. 304, Kluwer Academic Publishers, Dordrecht/Boston/London, 1996, pp. 257–270.
[57] J.J. Thomas, H.M. Jennings, A colloidal interpretation of chemical aging of the C–S–H gel and its effects on the properties of cement paste, Cem. Concr. Res. 36 (1) (2006) 30–38.
[58] H.M. Jennings, J.J. Thomas, J.S. Gevrenov, G. Constantinides, F.J. Ulm, Modeling the nanostructure of C–S–H gel, in: K. Scrivener, E. Gallucci (Eds.), Proc. of Int. Conf. ''Cementitious Materials as Model Porous Media: Nanostructure and Transport Processes'', july 17–22, 2005, Monte Verità, Switzerland, EPFL, Lausanne, 2005, pp. 79–85.
[59] G.W. Scherer, Structure and properties of gels, Cem. Concr. Res. 29 (1999) 1149–1157.
[60] Recommended test methods for measuring the parameters associated to durability (in French), Proc. of Journées Techniques AFPC-AFREM ''Durabilité des Bétons'', dec. 11–12, 1997, Toulouse, France, LMDC, Toulouse, 1998.
[61] V. Baroghel-Bouny, J. Godin, Experimental study on drying shrinkage of ordinary and high-performance cementitious materials, Concr. Sci. Eng. 3 (9) (2001) 13–22.
[62] E.P. Barrett, L.G. Joyner, P.P. Halenda, The determination of pore volume and area distributions in porous substances. I — Computations from nitrogen isotherms, J. Am. Chem. Soc. 73 (1951) 373–380.
[63] J.J.R. Hagymassy, S. Brunauer, R.SH. Mikhail, Pore structure analysis by water vapour adsorption — *t*-curves for water vapour, J. Colloid Interface Sci. 29 (3) (1969) 485–491.

[64] V. Baroghel-Bouny, T. Chaussadent, Pore structure and moisture properties of cement-based systems from water vapour sorption isotherms, in: S. Diamond, S. Mindess, F.P. Glasser, L.W. Roberts, J.P. Skalny, L.D. Wakeley (Eds.), Proc. of MRS 1994 Fall Meeting, nov. 28 – dec. 2, 1994, Boston, USA, vol. 370, Materials Research Society, Pittsburgh, 1995, pp. 245–254.
[65] V. Baroghel-Bouny, Texture and moisture properties of ordinary and high-performance cementitious materials, in: J.P. Bournazel, Y. Malier (Eds.), Proc. of Int. RILEM Conf. ''Concrete: from Material to Structure'', 11–12 sept., 1996, Arles, France, RILEM, Cachan, 1998, pp. 144–165.
[66] V. Baroghel-Bouny, T. Chaussadent, Texture and moisture characterization of hardened cement pastes and concretes from water vapour sorption measurements, in: H.M. Jennings, J. Kropp, K. Scrivener (Eds.), Proc. of NATO/RILEM Workshop on the Modelling of Microstructure and its Potential for Studying Transport Properties and Durability, july 10–13, 1994, Saint-Rémy-lès-Chevreuse, France, NATO ASI Series E: Applied Sciences, vol. 304, Kluwer Academic Publishers, Dordrecht/Boston/London, 1996, pp. 241–255.
[67] I. Odler, The BET-specific surface area of hydrated Portland cement and related materials, Cem. Concr. Res. 33 (2003) 2049–2056.
[68] I.G. Richardson, The nature of C–S–H in hardened cements, Cem. Concr. Res. 29 (8) (1999) 1131–1147.
[69] G.J. Verbeck, R.H. Helmuth, Structures and physical properties of cement paste (principal paper), Proc. of 5th Int. Congress on the Chemistry of Cement, Tokyo, Japan, Session III.1: Structures and Physical Properties of Cement Paste, vol. 3, Cement Association of Japan, Tokyo, 1968, pp. 1–32.
[70] J.J. Beaudoin, P.W. Brown, The structure of hardened cement paste, Proc. of 9th Int. Congress on the Chemistry of Cement, New Delhi, India, Theme III.C: Structural Models for Hydrated Cement Pastes, vol. 1, National Council for Cement and Building Materials, New Delhi, 1992, pp. 485–525.
[71] F.H. Wittmann, The structure of hardened cement paste — a basis for better understanding of the material properties, Proc. of Conf. ''Hydraulic Cement Pastes: their Structure and Properties'', Sheffield, U.K. Cement and Concrete Association, Sheffield, 1976, pp. 96–117.
[72] F. Barberon, J.-P. Korb, D. Petit, V. Morin, E. Bermejo, Probing the surface area of a cement-based material by nuclear magnetic relaxation dispersion, Phys. Rev. Lett. 90 (11) (2003) 116103–116104.
[73] D.N. Winslow, S. Diamond, Specific surface of hardened Portland cement paste as determined by Small-Angle X-ray Scattering, J. Am. Ceram. Soc. 57 (5) (1974) 193–197.
[74] J.J. Völkl, R.E. Beddoe, M.J. Setzer, The specific surface of hardened cement paste by small-angle X-ray scattering. Effect of moisture content and chlorides, Cem. Concr. Res. 17 (1987) 81–88.
[75] V. Baroghel-Bouny, T.Q. Nguyen, M. Thiery, P. Dangla, P. Belin, Evaluation and prediction of reinforced concrete durability by means of durability indicators. Part II: Multi-level predictive modelling, in: K. Kovler (Ed.), Proc. of Int. RILEM-JCI Seminar on Concrete Durability and Service Life Planning ''ConcreteLife′06'', March 14–16, 2006, Ein-Bokek, Dead Sea, Israel, RILEM Publications, Bagneux, 2006, pp. 270–280, PRO 46.
[76] R.A. Olson, H.M. Jennings, Estimation of C–S–H content in a blended cement paste using water adsorption, Cem. Concr. Res. 31 (2001) 351–356.
[77] P. Mounanga, A. Khelidj, A. Loukili, V. Baroghel-Bouny, Predicting Ca $(OH)_2$ content and chemical shrinkage of hydrating cement pastes using analytical approach, Cem. Concr. Res. 34 (2) (2004) 255–265.
[78] V.G. Papadakis, C.G. Vayenas, M.N. Fardis, Physical and chemical characteristics affecting the durability of concrete, ACI Mater. J. 88 (2) (1991) 186–196.
[79] V.G. Papadakis, Effect of supplementary cementing materials on concrete resistance against carbonation and chloride ingress, Cem. Concr. Res. 30 (10) (2000) 291–299.
[80] J.H. de Boer, B.C. Lippens, Studies on pore systems in catalysts, V — the *t*-method, J. Catal. (USA) 4 (1965) 319–323.
[81] J.P. Monlouis-Bonnaire, Numerical modelling of coupled air–water–salt transfers in cementitious materials and terracotta (in French), Ph.D dissertation, Toulouse, 2003, 213 p.
[82] B. Czernin, Cementkemi för Byggare, Svenska Cementforeningen, 1956.
[83] F.J. Ulm, G. Constantinides, F.H. Heukamp, Is concrete a poromechanics material? — a multiscale investgation of poroelastic properties, Mat. Struct./Concr. Sci. Eng. 37 (265) (2004) 43–58.
[84] V. Baroghel-Bouny, Evaluation and prediction of reinforced concrete durability by means of durability indicators. Part I: new performance-based approach, in: K. Kovler (Ed.), Proc of Int. RILEM-JCI Seminar on Concrete Durability and Service Life Planning ''ConcreteLife′06'', March 14–16, 2006, Ein-Bokek, Dead Sea, Israel, RILEM Publications, Bagneux, 2006, pp. 259–269, PRO 46.
[85] D.P. Bentz, Influence of water-to-cement ratio on hydration kinetics: simple models based on spatial considerations, Cem. Concr. Res. 36 (2) (2006) 238–244.